

## Pre-ALMA observations of GRBs in the mm/submm range<sup>★,★★</sup>

A. de Ugarte Postigo<sup>1,2</sup>, A. Lundgren<sup>3,4</sup>, S. Martín<sup>3</sup>, D. Garcia-Appadoo<sup>3,4</sup>, I. de Gregorio Monsalvo<sup>3,4</sup>, A. Peck<sup>4</sup>, M. J. Michałowski<sup>5</sup>, C. C. Thöne<sup>2</sup>, S. Campana<sup>6</sup>, J. Gorosabel<sup>2</sup>, N. R. Tanvir<sup>7</sup>, K. Wiersema<sup>7</sup>, A. J. Castro-Tirado<sup>2</sup>, S. Schulze<sup>8</sup>, C. De Breuck<sup>9</sup>, G. Petitpas<sup>10</sup>, J. Hjorth<sup>1</sup>, P. Jakobsson<sup>8</sup>, S. Covino<sup>6</sup>, J. P. U. Fynbo<sup>1</sup>, J. M. Winters<sup>11</sup>, M. Bremer<sup>11</sup>, A. J. Levan<sup>12</sup>, A. Llorente<sup>13</sup>, R. Sánchez-Ramírez<sup>2</sup>, J. C. Tello<sup>2</sup>, and R. Salvaterra<sup>14</sup>

<sup>1</sup> Dark Cosmology Centre, Niels Bohr Institute, Juliane Maries Vej 30, 2100 Copenhagen Ø, Denmark  
e-mail: adeugartepostigo@gmail.com

<sup>2</sup> Instituto de Astrofísica de Andalucía (IAA-CSIC), Glorieta de la Astronomía s/n, 18008 Granada, Spain

<sup>3</sup> European Southern Observatory, Vitacura Casilla 19001, Santiago de Chile 19, Chile

<sup>4</sup> Joint ALMA Observatory, Alonso de Córdova 3107, Vitacura – Santiago, Chile

<sup>5</sup> Scottish Universities Physics Alliance, Institute for Astronomy, University of Edinburgh, Royal Observatory, Edinburgh, EH9 3HJ, UK

<sup>6</sup> INAF – Osservatorio Astronomico di Brera, via E. Bianchi 46, 23807 Merate (LC), Italy

<sup>7</sup> Department of Physics and Astronomy, University of Leicester, University Road, Leicester LE1 7RH, UK

<sup>8</sup> Centre for Astrophysics and Cosmology, Science Institute, University of Iceland, Dunhagi 5, 107 Reykjavík, Iceland

<sup>9</sup> European Southern Observatory, Karl Schwarzschild Straße 2, 85748 Garching, Germany

<sup>10</sup> Harvard-Smithsonian Center for Astrophysics, Submillimeter Array, 645 North A'ohoku Place, Hilo, HI 96720, USA

<sup>11</sup> Institut de Radioastronomie Millimétrique (IRAM), 300 rue de la Piscine, 38406 Saint Martin d'Hères, France

<sup>12</sup> Department of Physics, University of Warwick, Coventry, CV4 7AL, UK

<sup>13</sup> Herschel Science Operations Centre, INSA, ESAC, Villafraanca del Castillo, 50727, 28080 Madrid, Spain

<sup>14</sup> INAF/IASF Milano, via E. Bassini 15, 20133 Milano, Italy

Received 8 August 2011 / Accepted 12 December 2011

### ABSTRACT

**Context.** Gamma-ray bursts (GRBs) generate an afterglow emission that can be detected from radio to X-rays during days, or even weeks after the initial explosion. The peak of this emission crosses the millimeter and submillimeter range during the first hours to days, making their study in this range crucial for constraining the models. Observations have been limited until now due to the low sensitivity of the observatories in this range. This situation will be greatly improved with the start of scientific operations of the Atacama Large Millimeter/submillimeter Array (ALMA).

**Aims.** In this work we do a statistical analysis of the complete sample of mm/submm observations of GRB afterglows obtained before the beginning of scientific operations at ALMA.

**Methods.** We present observations of 11 GRB afterglows obtained from the Atacama Pathfinder Experiment (APEX) and the Submillimeter Array (SMA), as well as the first detection of a GRB with ALMA, still in the commissioning phase, and put them into context with a catalogue of all the observations that have been published until now in the spectral range that is covered by ALMA.

**Results.** The catalogue of mm/submm observations collected here is the largest to date and is composed of 102 GRBs, of which 88 have afterglow observations, whereas the rest are host galaxy searches. With our programmes, we contributed with data of 11 GRBs and the discovery of 2 submm counterparts. In total, the full sample, including data from the literature, has 22 afterglow detections with redshifts ranging from 0.168 to 8.2. GRBs have been detected in mm/submm wavelengths with peak luminosities spanning 2.5 orders of magnitude, the most luminous reaching  $10^{33}$  erg s<sup>-1</sup> Hz<sup>-1</sup>. We observe a correlation between the X-ray brightness at 0.5 days and the mm/submm peak brightness. Finally we give a rough estimate of the distribution of peak flux densities of GRB afterglows, based on the current mm/submm sample.

**Conclusions.** Observations in the mm/submm bands have been shown to be crucial for our understanding of the physics of GRBs, but have until now been limited by the sensitivity of the observatories. With the start of the operations at ALMA, the sensitivity has improved by more than an order of magnitude, opening a new era in the study of GRB afterglows and their host galaxies. Our estimates predict that, once completed, ALMA will detect up to ~98% of the afterglows if observed during the passage of the peak synchrotron emission.

**Key words.** gamma-ray burst: general – submillimeter: general

\* This publication is partially based on data acquired with the Atacama Pathfinder Experiment (APEX) under programmes 082.F-9850, 084.D-0732, 086.D-0590, 086.F-9303(A) and 087.F-9301(A) and with the Submillimeter Array (SMA) under programmes 2009B-S015, 2010A-S004 and 2010B-S026. This paper makes use of the following ALMA Science Verification data: ADS/JAO.ALMA#2011.0.00006.SV.

\*\* Table 1 is available in electronic form at

<http://www.aanda.org>

### 1. Introduction

Gamma-ray bursts (GRBs) are the brightest explosions in the Universe, releasing isotropic equivalent energies in the range of  $10^{51}$ – $10^{54}$  erg (of the order of  $10^{51}$  erg once corrected for collimation) within a few seconds. They were serendipitously discovered in 1967 (Klebesadel et al. 1973) in gamma-rays, but

it was not until 1997 that the first counterparts were detected at other wavelengths (van Paradijs et al. 1997; Frail et al. 1997; Costa et al. 1997; Bremer et al. 1998). Thanks to the observation of the fading X-ray emission, which follows the more energetic gamma-ray photons, and the rapid distribution of the X-ray coordinates (much more precise than the gamma-ray ones), it is possible to carry out multiwavelength observations of the counterparts associated with GRBs within seconds of their occurrence. The late time emission, detectable at all wavelengths and observable for days after the burst onset (and some times significantly longer), is what we call GRB *afterglow*.

It is widely accepted that long GRBs (those with durations above  $\sim 2$  s) are related to the collapse of massive stars (Woosley 1993; Paczyński 1998; Hjorth et al. 2003) while short GRBs (shorter than  $\sim 2$  s) are probably originated by the coalescence of two compact objects, such as two neutron stars or a neutron star and a black hole (Paczynski 1990; Narayan et al. 1992; Levan et al. 2006; Chattopadhyay et al. 2007; King et al. 2007). In both scenarios, the result is the ejection of material at ultrarelativistic speeds, most probably through jets. This is what we call the *relativistic fireball model* (Rees & Meszaros 1992; Sari et al. 1998). In this framework, a compact source releases  $\sim 10^{51}$  erg of energy within dozens of seconds in a region smaller than 10 km. When the ejecta run into the surrounding medium, a forward shock sweeps the surroundings of the progenitor, producing an afterglow as the ejecta interact with the interstellar matter. A reverse shock, colliding with the ejecta, can also produce an additional emission during early times (Piran 1999).

Until now, millimeter and especially submillimeter observations of GRBs have been scarce due to the small number of available observatories and limited sensitivity, as compared to other wavelength ranges. As examples of large samples of afterglow data see, for example, Evans et al. (2009) in X-rays, Kann et al. (2010) in optical, and more recently Chandra & Frail (2012) in radio. The mm/submm range suffers strongly from atmospheric absorption, mostly due to water vapour. This means that observatories have to be placed in high and dry mountain sites. Nevertheless, the study of GRBs in these wavelengths is of great interest, as the peak (in flux density) of the synchrotron afterglow emission, and even the one due to the reverse shock (see Sect. 3.1 for a description of the emission mechanisms), is expected to be located in this wavelength range during the first days. It has also the benefit of being a wavelength range that is not affected by interstellar extinction, as are the optical or soft X-rays, allowing us to detect highly-extinguished and high-redshift bursts. This range is also normally above the self-absorption frequency of the spectrum, below which the flux is strongly suppressed. Finally, as compared to centimeter and decimeter wavelengths, this range is not affected by interstellar scintillation, allowing more accurate modelling with fewer observations.

Pioneering submm observations of GRB afterglows, made with JCMT/SCUBA (e.g. Smith et al. 1999, 2001) in the submm and with various facilities in the mm (e.g. Bremer et al. 1998; Galama et al. 2000), showed that emission in these wavelengths could be detected in some cases, and provided the first tests of the fireball model using full radio to X-ray SEDs (e.g. Wijers & Galama 1999). However, detections were generally of low significance, and progress in the *Swift* era was restricted until recently by the dearth of submm bolometer array instruments (following the retirement of SCUBA on JCMT, and until the advent of LABOCA on APEX).

On the 30th September 2011 ALMA came into operation, to revolutionise mm/submm astronomy. ALMA is at an altitude of 5000 m in the Llano de Chajnantor, in northern Chile, one of the

best sites for this kind of observations in the world. In its early science phase it has 16 antennas of 12 m, and in full operations (expected for 2013) it will increase to a total of 50 antennas of 12 m in diameter plus a compact array (the Atacama Compact Array – ACA) of 12 7 m antennas and four 12 m antennas. This will be the largest facility for mm/submm astronomy and will improve sensitivity and spatial resolution in over an order of magnitude with respect to previous observatories.

In this paper we collect all the data, to our best knowledge, that have been published for GRBs in the mm/submm range, to which we add observations from our observing programmes from APEX and the SMA. The observations are completed with the first ALMA observation of a GRB, during the commissioning phase of the observatory, as a test of the target of opportunity procedures. Using this sample, we give a review of the past experience and put it into context of the forthcoming ALMA era. We give some examples of single-epoch spectral energy distributions but do not attempt full broadband modelling for individual bursts as it is beyond the scope of this paper.

Section 2 describes the data of 11 bursts collected with our observing programmes. Section 3 presents the catalogue of mm/submm GRB data. In Sect. 4 we describe the capabilities of ALMA compared with previous observatories and discuss its future role in the field. Finally, Sect. 5 lists our conclusions. Throughout the paper we assume a cosmology with  $\Omega_m = 0.30$ ,  $\Omega_\Lambda = 0.70$ , and  $H_0 = 70$ .

## 2. Observations

On March 2009 we performed the first observation of a GRB (GRB 090313) using the 12 m, single-dish, APEX telescope (in Chajnantor, Chile; Güsten et al. 2006) at 345 GHz, as a feasibility test, during a technical night through a Director Discretionary Time programme. Since then, we have had several observing programmes at APEX, with which we have followed-up 6 GRBs (plus an additional Galactic X-ray binary, initially identified as a GRB). All these observations were performed using the Large Apex Bolometer Camera (LABOCA; Siringo et al. 2009), a multi-channel bolometer array with 295 elements designed for continuum observations, with a field of view (FOV) of  $11'.4 \times 11'.4$  and an angular resolution of  $19.5 \pm 1''$ . Observations until the end of 2009 were performed using a spiral raster mapping, whereas later observations used the photometric mode. The mapping mode results in a fully sampled and homogeneously covered map which is less sensitive than the photometric mode (which lacks the spatial resolution) that was made available in 2010. We chose to use the photometric mode when it became available, as we are more interested in the sensitivity than in the spatial coverage, as our sources are unresolved. Data reduction of LABOCA/APEX observations was done using BoA<sup>1</sup>, as well as CRUSH and miniCRUSH (Kovács 2008) software packages.

Since November 2009 we have an observing project for GRB afterglows from the northern hemisphere at the 8-antenna SMA interferometer (Hawaii, USA) with which we have followed-up 4 other bursts. Observations from SMA were reduced using the MIR-IDL<sup>2</sup> and MIRIAD (Sault et al. 1995) packages.

In the following, we provide details on each of our GRB observations. The data are listed, together with the complete catalogue in Table 1.

<sup>1</sup> [http://www.mpifr-bonn.mpg.de/div/submmtech/software/boa/boa\\_main.html](http://www.mpifr-bonn.mpg.de/div/submmtech/software/boa/boa_main.html)

<sup>2</sup> <https://www.cfa.harvard.edu/~cqj/mircook.html>

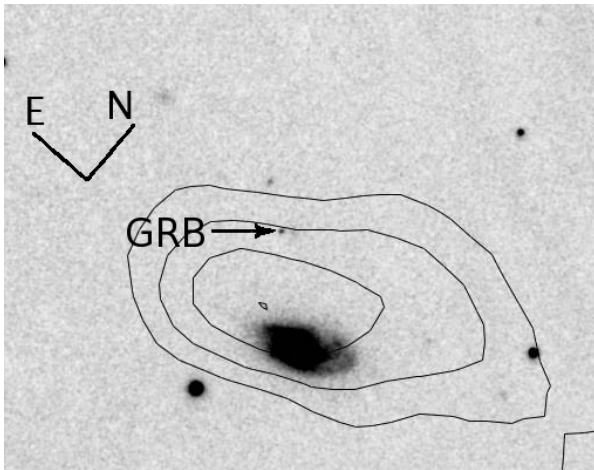


**Fig. 1.** Observation of GRB 090313 with APEX (contours are 1, 2, 3 and  $4\sigma$  detection levels) in March 2009 plotted over an optical X-shooter acquisition image showing the position of the afterglow. The field of view is  $90'' \times 70''$ . Only a field galaxy, unassociated with the GRB is detected, and we impose a 3-sigma upper limit of 9 mJy for the afterglow (adapted from de Ugarte Postigo et al. 2010c; Melandri et al. 2010).

**GRB 090313:** This burst was a 78 s long event with a bright afterglow at a redshift of  $z = 3.3736$  (de Ugarte Postigo et al. 2010c). After the discovery of a bright mm counterpart (Bock et al. 2009a), we obtained continuum observations at 345 GHz using LABOCA/APEX bolometer array during technical time. Data were acquired on 2009 March 17 and 24 under good weather conditions (zenith opacity values ranged from 0.24 to 0.33 at 345 GHz). Observations were performed using a spiral raster mapping, providing a fully sampled and homogeneously covered map in an area of diameter  $12'$ , centered at the coordinates of the optical afterglow of GRB 090313. The total on-source integration time of the two combined epochs was 4.6 h. Calibration was performed using observations of Saturn as well as IRAS 09452+1330, HD 82385, G10.6-0.4, and IRAS 17574-2403 as secondary calibrators. The absolute flux calibration uncertainty is estimated to be 11%. The telescope pointing was checked every hour, finding a root mean square (rms) pointing accuracy of  $1''.8$ . The individual maps were co-added and smoothed to a final angular resolution of  $27''.6$ . We obtained a  $3\sigma$  upper limit of 14 mJy for each of the two epochs and a limit of 9 mJy in the coadded maps (see Fig. 1). These data were presented, together with an analysis of the evolution of the afterglow emission by Melandri et al. (2010).

**GRB 091102:** This was the first burst that we observed during our regular programme time. It was a 6.6 s long burst, for which no credible optical counterpart was identified and no redshift was obtained. LABOCA/APEX observations were performed on 2009 November 3 under average weather conditions (zenith opacity values ranged from 0.4 to 0.5 at 345 GHz). The total on-source integration time was  $\sim 2$  h. Calibration was performed using observations of Uranus and Neptune. The absolute flux calibration uncertainty is estimated to be  $\sim 8\%$ . The telescope pointing was checked every hour towards the source PMNJ0450-8100. We obtained a  $3\sigma$  point source sensitivity of 20 mJy.

**GRB 091127:** This was a nearby burst ( $z = 0.49044$ ; Vergani et al. 2011) with a duration of 7.1 s and a bright optical counterpart that we followed with LABOCA/APEX on 2009 Nov. 28 and 29 at 345 GHz. Weather conditions were average, with zenith opacity values ranging from 0.4 to 0.63 at 345 GHz.

Observations were performed using a spiral raster mapping. The total on-source integration time of the two combined epochs was 6.4 h (2.9 and 3.5 h in the first and second epoch, respectively). Pointing was checked regularly on J0050-095 and J0145-276. Calibration was performed using observations of Uranus and the secondary calibrator NGC 2071 IR. The absolute flux calibration uncertainty is estimated to be about 15%. We obtained  $3\sigma$  upper limits of 14.9 mJy and 13.2 mJy for each of the two epochs, respectively, and 9.6 mJy for the combined epochs. An analysis of the afterglow emission of this burst, including the APEX data, is presented by Vergani et al. (2011).

**GRB 100418A:** On April, 18th 2010, the *Swift* Burst Alert Telescope (BAT) triggered and located GRB 100418A. It was an intermediate duration burst (7.0 s) at a redshift of  $z = 0.62$  (Antonelli et al. 2010). It had a peculiar optical light curve peaking several hours after the event. We performed observations of the afterglow using 7 out of the 8 SMA antennas, starting  $\sim 16$  h after the burst. Weather conditions were good, with zenith opacities at 225 GHz of  $\tau \sim 0.06$  (precipitable water vapour, PWV  $\sim 1$  mm). Titan and Neptune were used as flux calibrators and 3C 454.3 as bandpass calibrator. Atmospheric gain was corrected from observations of the nearby quasar J1751+096 every 15 min. Using these data we discovered a bright counterpart (Martin et al. 2010) at a flux of  $13.40 \pm 1.60$  mJy (see Fig. 2). At the time of the discovery, this was the second brightest mm/submm counterpart detected (after GRB 030329, which peaked at  $\sim 70$  mJy; Sheth et al. 2003; Resmi et al. 2005). Observations continued over the following 4 nights, tracking the evolution of the afterglow until it became undetectable on April 23rd (de Ugarte Postigo et al., in prep.).

**GRB 100814A:** This was a very long burst (150 s) with a bright counterpart at a redshift of  $z = 1.44$  (O'Meara et al. 2010). Continuum observations at 345 GHz were carried out using LABOCA/APEX. Data were acquired on August 15, 2010, starting 26 h after the burst, under good weather conditions (zenith opacity value was 0.28 at 345 GHz). Observations were performed using the photometry mode. The total on-source integration time was 1.5 h. Pointing was checked regularly on J0145-276. Calibration was performed using observations of Uranus and the secondary calibrator V883-ORI. The absolute flux calibration uncertainty is estimated to be about 15%. The formal flux measured at the position of the afterglow was  $-0.33 \pm 1.6$  mJy/beam, i.e. a  $3\sigma$  limit of 4.8 mJy. A radio counterpart was detected by Chandra et al. (2010) several days later from EVLA.

**GRB 100901A:** This was a bright event, at a redshift of  $z = 1.41$  (Chornock et al. 2010). Observations were carried out with SMA on the 3rd of September 2010. All eight antennas, arranged in the extended array configuration, were tuned to 345.8 GHz. Weather was excellent with a zenith opacity at 225 GHz of  $\tau \sim 0.06$  (precipitable water vapour, PWV  $\sim 1$  mm). Uranus and Callisto were observed as flux calibrators and 3C 454.3 as bandpass. Atmospheric gain calibration was derived from the observations of the nearby quasars J0237+288 and J0319+415 every 15 min. The GRB was observed for  $\sim 10$  h, and the observations resulted in a non detection, being the GRB flux constrained down to an rms noise of  $\sim 0.75$  mJy, which gives the deepest limit in our sample. A radio counterpart was later detected by WSRT (van der Horst et al. 2010c,b) and EVLA (Chandra & Fraile 2010).

**GRB 100925A/MAXI J1659-152:** On 2010 September 25 we responded to a GRB alert using APEX. Observations were performed 15.5 h after the burst onset and a bright submillimeter afterglow was detected, with a flux density of

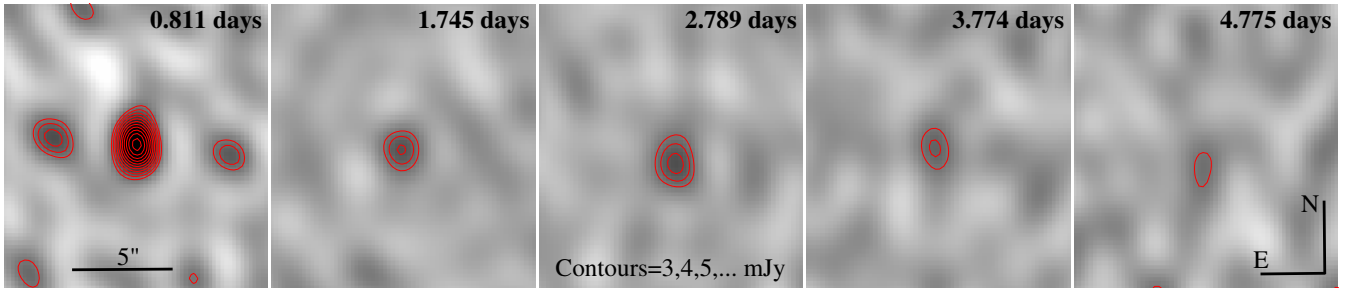


**Fig. 2.** Observations of GRB 100418A obtained with SMA during the first 5 days after the GRB (adapted from de Ugarte Postigo et al., in prep.).

$12.6 \pm 2.4$  mJy (de Ugarte Postigo et al. 2010d). Later spectroscopic observations performed with the X-shooter spectrograph at the Very Large Telescope, showed that the source was not due to an extragalactic GRB but to an unusually energetic burst from an X-ray binary (de Ugarte Postigo et al. 2010b). Thanks to the detection from APEX, an extensive radio observation campaign was triggered (van der Horst et al. 2010a, including further observations from APEX).

**GRB 110422A:** Observations of this burst at  $z = 1.770$  (Malesani et al. 2011; de Ugarte Postigo et al. 2011a) were carried out with the SMA on May 6th, 2011 in search for an emission tentatively detected by the *Herschel* Space Observatory (Huang et al. 2011). The seven available antennas were tuned to 233.7 GHz. Weather was bad but stable enough with zenith opacity at 225 GHz was  $\tau \sim 0.35$  (PWV > 5 mm). J0721+713 was used as flux calibrator and 3C 273 as bandpass. Atmospheric gain calibration was derived from J0721+713 quasar observations every 15 min. The GRB was observed for 4 h, reaching an rms noise of  $\sim 2.8$  mJy but obtained no detection.

**GRB 110503A:** Observations of this  $z = 1.613$  (de Ugarte Postigo et al. 2011b) burst were carried out with the SMA on May 4th, 2011. The five available antennas were tuned to 225.0 GHz. Weather was mediocre but stable with zenith opacity at 225 GHz was  $\tau \sim 0.25$  (PWV > 4 mm). J0927+390 was used as flux calibrator and 3C 273 as bandpass. Atmospheric gain calibration was derived from J0927+390 and J0920+446 quasar observations every 15 min. The GRB was observed for 7 h reaching an rms noise of  $\sim 1.7$  mJy.

**GRB 110709B:** This was a very peculiar burst, that showed two gamma-ray triggers over a period of almost 15 min (Barthelmy et al. 2011). Early optical observations showed that it was a very dark event (Fong & Berger 2011), with no credible afterglow detected or redshift measured. We performed submm observations with APEX to try to localise the counterpart and to constrain the synchrotron spectrum. Observations began on July 11, 2.00 days after the burst, with an on-source time of 106 min and precipitable water vapour of 0.8 mm. We did not detect any significant emission, obtaining a formal flux on the source position of  $1.4 \pm 2.3$  mJy (3-sigma limit of 6.9 mJy). A detection of a radio counterpart at 5.8 GHz was later reported by Zauderer & Berger (2011).

**GRB 110715A:** This burst had a very bright optical counterpart in spite of being located very close to the plane of the Milky Way from which it suffered from significant dust extinction. Its redshift was measured to be  $z = 0.82$  (Piranomonte et al. 2011). APEX observations began on July 16, 1.42 days after the burst and were performed using the photometric mode. The weather conditions were very good, with a precipitable water vapor of 0.62 mm. Using these observations we discovered a bright submm counterpart at  $10.4 \pm 2.4$  mJy (de Ugarte Postigo et al. 2011e).

As a test of the target of opportunity procedure, GRB 110715A was subsequently observed at Atacama Large Millimeter Array (ALMA). The ALMA Science Team report a preliminary detection from a test observation of this source of  $4.9 \pm 0.6$  mJy at 345 GHz after 25 min on source with 7 antennas. The centroid of the ALMA position is 15:50:44.05–46:14:06.54 with an uncertainty of  $0'.3 \times 0'.1$  at a position angle of 76 degrees. Observations began on July 19 at 02:50 UT (3.57 days after the burst). The weather conditions were very good, with a precipitable water vapor of 0.5 mm. In spite of being obtained during a test observation, with an order of magnitude fewer antennas than will be available with the full observatory and for only 25 min, this is the deepest observation in the complete sample at 345 GHz and provides the most accurate coordinates available for this burst. A complete analysis of the afterglow emission of this burst, will be presented by Sanchez-Ramirez et al. (in prep.).

**GRB 110918A:** This burst, at a redshift of  $z = 0.98$  (Levan et al. 2011) was one of the brightest GRBs ever detected in gamma-rays, and the brightest ever observed by Konus/WIND (Golenetskii et al. 2011). The large error box generated just with Konus/WIND data did not allow us to observe until 2 days after, when the coordinates were refined thanks to the detection of X-ray (Mangano et al. 2011) and optical counterparts (Tanvir et al. 2011). Continuum observations at 345 GHz were carried out using LABOCA/APEX. Data were acquired on 2011-09-21 between 03:02 and 05:46 under excellent conditions (zenith opacity value was 0.2 at 345 GHz). Observations were performed using the photometry mode. The total on source integration time was 2.41 h. Pointing was checked regularly on J0145-276. Calibration was performed using observations of Uranus and Neptune and the secondary calibrator V883-ORI. The absolute flux calibration uncertainty is estimated to be about 15%. Because of technical issues, the data did not reach the theoretical noise level, being no flux measured at the position of the afterglow and the upper 3- $\sigma$  limit was 15 mJy.

### 3. The pre-ALMA millimeter/submillimeter sample of GRBs

In order to put our observations into context, we have collected, in Table 1, the most complete sample of continuum observations that have been published to date of GRB afterglows and their host galaxies in the ALMA wavelength range, covering from early 1997 until the 30th of September 2011 (starting day of the early science operations with ALMA). The data are ordered chronologically by GRB, considering as detections only those with higher significance than  $3\sigma$ , and otherwise providing detection limits. The observations are separated into ALMA bands 3 (84–116 GHz), 4 (125–163 GHz), 6 (211–275 GHz), 7 (275–373 GHz) and 9 (602–720 GHz). See Table 2

**Table 2.** Definition of the ALMA bands.

Band	Frequency range (GHz)	Wavelength range (mm)
Band 1	31–45	6.66–9.67
Band 2	67–90	3.33–4.47
<b>Band 3</b>	<b>84–116</b>	<b>2.58–3.56</b>
Band 4	125–163	1.84–2.40
Band 5	162–211	1.42–1.85
<b>Band 6</b>	<b>211–275</b>	<b>1.09–1.42</b>
<b>Band 7</b>	<b>275–373</b>	<b>0.80–1.09</b>
Band 8	385–500	0.60–0.78
<b>Band 9</b>	<b>602–720</b>	<b>0.42–0.50</b>
Band 10	787–950	0.32–0.38

**Notes.** The four marked in bold will be the main observing bands and the only ones offered for early science.

**Table 3.** Detection ratios in the catalogue for each of the observing bands, considering only  $3\sigma$  or higher significance detections.

	Afterglows	Host galaxies
Band 3	18/61 (30%)	0/3 (0%)
Band 4	1/2 (50%)	–
Band 6	6/38 (16%)	2/8 (25%)
Band 7	5/31 (16%)	3/27 (11%)
Band 9	0/6 (0%)	0/15 (0%)
Total	22/88 (25%)	4/36 (11%)

**Notes.** For host galaxies we consider only dedicated searches and not the limits derived from afterglow searches.

for a definition of all the ALMA bands<sup>3</sup>, which we will use throughout the paper for simplicity. The complete sample includes observations of 102 bursts. There have been 88 searches for GRB afterglows, of which 22 have reports of detections. Separating into individual bands, we have 18 detections in band 3, one in band 4, six in band 6, five in band 7 and none in band 9. Table 3 displays a list of the detection ratios for each of the observing bands. As for the host galaxies, there have been specific host galaxy searches for 36 cases, although limits can be provided for the 102 bursts that have been followed. Host galaxy detections have only been achieved in four cases: GRB 000210, GRB 000418, GRB 010222 and XT 080109, this last one cannot be considered a normal GRB as the burst was in X-rays and not in gamma (Soderberg et al. 2008). There have been further claims of host detections but we consider only those with signal to noise ratio greater than 3.

Figure 3 shows a compilation of the mm/submm GRB afterglow light curves for ALMA bands 3, 6 and 7. Figure 4 shows histograms of the peak detections and detection limits. The peak detections are, strictly speaking, only lower limits to the peak flux density in each band, as only a few light curves cover the maximum of the light curve. The detection limits are the single-epoch deepest  $3\sigma$  limits for each burst, independently of the time of the observation, so they can only be indicative of the capabilities of pre-ALMA observatories.

The afterglow peak flux for each observing band in the mm/submm range is expected to be very similar, with only the time at which the peak is reached being different. According to the fireball model (Sari et al. 1998, see also Sect. 3.1), the peak is expected to cross from higher to lower energies, so that the higher frequency bands are expected to peak first. Hence, the

<sup>3</sup> Adapted from <http://www.almaobservatory.org>

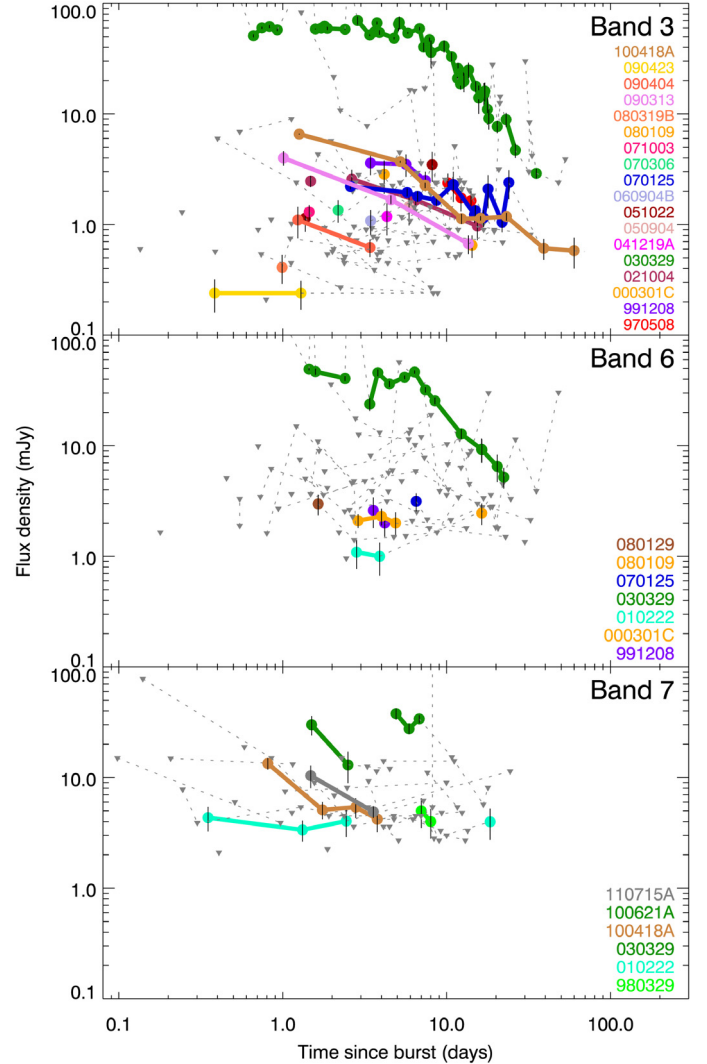


**Fig. 3.** Light curves of GRB afterglows in the different bands (see Table 2 for a definition of the bands). Coloured dots indicate detections, while gray triangles are  $3\sigma$  detection limits. Observations of an individual burst are connected by a thick coloured line in case of detections and a thin dotted line in case of detection limits. GRBs with only one observation are shown as individual symbols with no connecting lines. Detections of GRB 010222 in bands 6 and 7 are due to the host galaxy and not the afterglow. The detection of XT 080109 in band 6 is due to the host galaxy.

ratio of afterglow detections is mostly determined by the different observing sensitivities of each of the telescopes in each band, given a reasonably prompt reaction time. Table 4 displays the median time between the burst onset and the first observation for the bursts in the sample, together with the median  $3\sigma$  limiting flux of the earliest observations. We do not include Band 4, as it has only 2 observations and the statistics are not significant.

### 3.1. The physics of GRBs and their environments

GRB afterglows can be described, in the simplest case, using the fireball model (Sari et al. 1998). According to this model, material is ejected at ultrarelativistic velocities through collimated jets (with opening angle  $\theta_j$ ). When this material interacts with the medium surrounding the progenitor, the accelerated particles emit a synchrotron spectrum that is characterised by three break frequencies:  $\nu_m$  is the characteristic synchrotron frequency

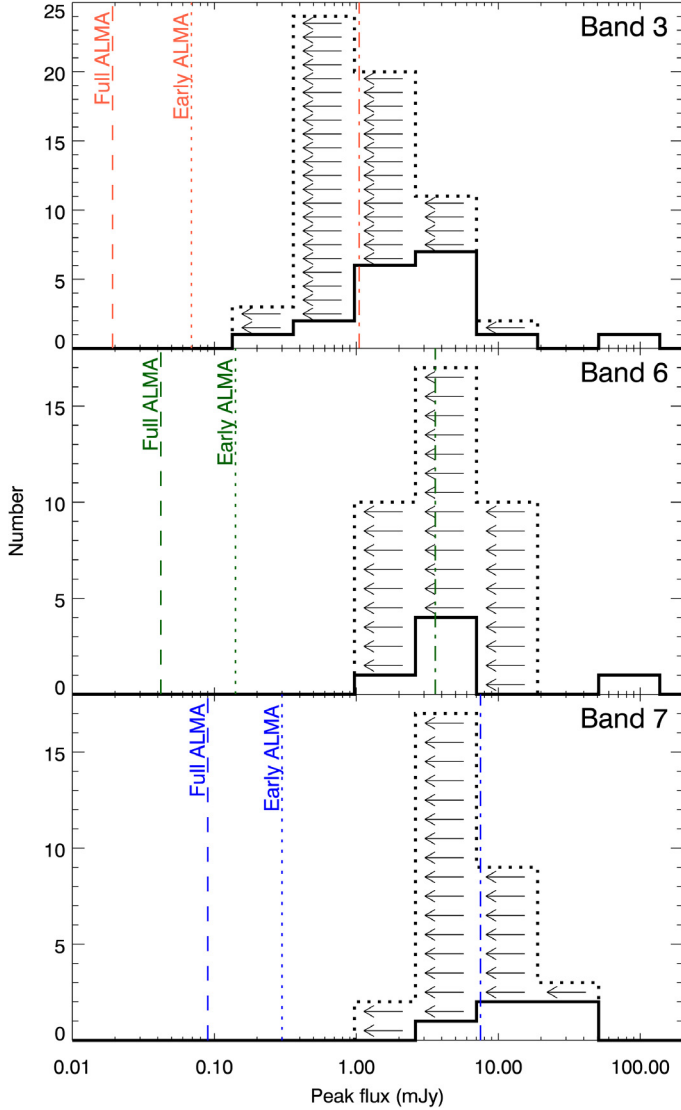


**Fig. 4.** Histograms of peak fluxes and  $3\sigma$  upper limits in each of the three main bands in our sample. Detection limits for early and full ALMA ( $3\sigma$ , derived from the rms calculated in Table 5) are indicated with vertical dotted and dashed lines, respectively. The dashed-dotted line indicates the median detection limit of the early observations (see Table 4).

**Table 4.** Median time between the burst and the first observation in each band and median limiting flux of those first observations ( $3\sigma$ ).

	Time (day)	Limiting flux (mJy)
Band 3	2.59	0.87
Band 6	2.67	3.87
Band 7	2.06	7.50
Band 9	4.47	60.0

and is the maximum of the emission;  $\nu_c$  is the cooling frequency, above which radiative cooling is significant;  $\nu_a$  is the synchrotron self-absorption frequency.

The location of the spectral breaks at a given time, and the spectral slopes, shown in Fig. 5, are determined by the following five parameters:  $E$  – isotropic equivalent kinetic energy of the shock;  $n$  – particle number density in the surroundings of the GRB, which can be considered constant or following a stellar

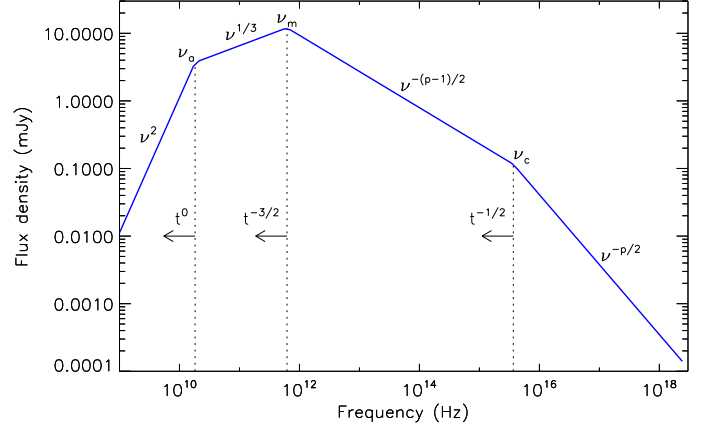


**Fig. 5.** The synchrotron afterglow spectrum expected from a simple fireball model in the slow-cooling regime, assuming a constant density environment and spherical expansion. The figure shows the characteristic frequencies, their evolution and the spectral slopes of the spectrum (adapted from Sari et al. 1998).

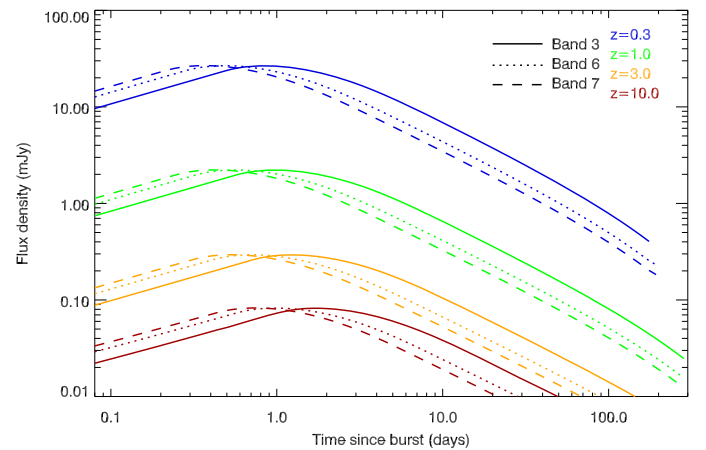


**Fig. 6.** Light curves of what could be a typical GRB afterglow using the standard fireball model, plotted for the different ALMA bands and at different redshifts.

wind profile;  $\epsilon_B$  – fraction of the shock energy that goes into magnetic energy density;  $\epsilon_e$  – fraction of the shock energy that goes to electron acceleration;  $p$  – slope of the relativistic electron energy distribution in the shock. Detailed multi-wavelength modelling of the spectral energy distribution allows us to derive these micro- and macro-physical parameters of the emission.

Figure 6 shows an example of what we would expect the light curves of a typical GRB to look like in the different ALMA bands and at different redshifts using the standard fireball model. It assumes an homogeneous jet, adiabatic dynamics (based on Rhoads 1999), constant density environment, and integration over equal arrival time surfaces. The physical parameters of the fireball are the following:  $E = 10^{53}$  ergs $^{-1}$ ,  $n = 0.1$  cm $^{-3}$ ,  $\epsilon_B = 0.01$ ,  $\epsilon_e = 0.088$ ,  $p = 2.1$  and  $\theta_j = 5$  deg. The light curves are characterised by a shallow rise during the first hours to days after the burst followed by a decay, as seen in most of the light curves of Fig. 3, when there are enough data points. The figure also shows how the peak is reached later at lower frequencies for a given redshift, while it is delayed for high redshift events due to cosmological time dilation.

A reverse shock, produced inside the ejecta, can produce additional emission at early times (Piran 1999). This emission has

been rarely observed in the optical wavelengths (e.g. Akerlof et al. 1999; Blake et al. 2005; Jelínek et al. 2006; Racusin et al. 2008; Zheng et al. 2011) but is expected to have a significant contribution in the early mm/submm emission (Inoue et al. 2007). For example, the mm detection of GRB 090423, at a redshift of 8.2, seems to show excess emission possibly due to a reverse shock (Castro-Tirado et al. 2009b; Chandra et al. 2010).

This model is, however, known to be too simplistic to explain the complex evolution that we can see in the densely sampled X-ray and optical light curves of *Swift* GRBs. Several modifications have been suggested to explain some of the observed fluctuations, flares, bumps and wiggles. Such modifications may include different density profiles and fluctuations (Wang & Loeb 2000; Ramirez-Ruiz et al. 2001; Dai & Lu 2002; Nakar & Piran 2003), energy injections (Rees & Meszaros 1998; Sari & Mészáros 2000; Granot et al. 2003; Björnsson et al. 2004; Jóhannesson et al. 2006), jets with complex structure (Mészáros et al. 1998; Kumar & Piran 2000; Rossi et al. 2002), late engine activity (Dai & Lu 1998; Zhang & Mészáros 2002; Ramirez-Ruiz 2004), microlensing (Loeb & Perna 1998; Garnavich et al. 2000; Ioka & Nakamura 2001) or dust echoes (Esin & Blandford 2000; Mészáros & Gruzinov 2000; Reichart 2001). Discerning the different scenarios is only possible through the analysis of the SEDs obtained with multi-wavelength observations (see Sect. 4) and, in some cases, with the aid of polarimetry.

### 3.2. Redshift distribution and luminosities

In spite of the strong limitation imposed by the detection limits of current observatories, the sample includes detections of GRBs at most redshifts, ranging from  $z = 0.168$  (GRB 030329 Greiner et al. 2003) all the way up to  $z = 8.2$  (GRB 090423 Tanvir et al. 2009; Salvaterra et al. 2009). XT 080109 at a redshift of 0.0065 (Malesani et al. 2008) had no gamma-ray emission, so we will exclude it from the analysis. This shows that GRBs can be great tools to study the evolution of the star formation across the complete history of the Universe also in this frequency range. Figure 7 shows the distribution of the redshifts of GRBs detected in the mm/submm range as compared to the distribution obtained from optical observations (Jakobsson et al. 2012). The mm/submm sample has a larger percentage of low redshift detections but, on the other hand, the average redshift was compensated by deep searches of the high redshift events. We note that the optical sample has its own biases, for example the limited capability to detect dark bursts (see Sect. 4.1 for a definition of dark burst). A Kolmogorov-Smirnov test gives a probability of 11% for both mm/submm detected bursts and the *Swift* sample of GRBs with redshift of coming from the same population. We obtain a median (mean) redshift for our sample of detections of 1.48 (1.99), as compared to 1.92 (2.19) of the sample of *Swift* bursts (Jakobsson et al. 2012).

In Fig. 8 we show the peak flux density measured in the mm/submm range as a function of the redshift. The dotted lines indicate the expected flux at different redshifts for objects of equal peak luminosities. The figure shows that the brightest burst ever detected, GRB 030329 (Hjorth et al. 2003; Stanek et al. 2003; Lipkin et al. 2004; Sheth et al. 2003; Resmi et al. 2005), is mainly so due to its low redshift. GRB 090423, the furthestmost detected in mm/submm, at a redshift of  $z = 8.2$  (Salvaterra et al. 2009; Tanvir et al. 2009), was not extremely luminous, and was only detected thanks to very deep observations (it is, in fact, the deepest detection in the sample; Castro-Tirado et al., in prep.). GRB 080319B, also known as the “naked-eye burst” due to its

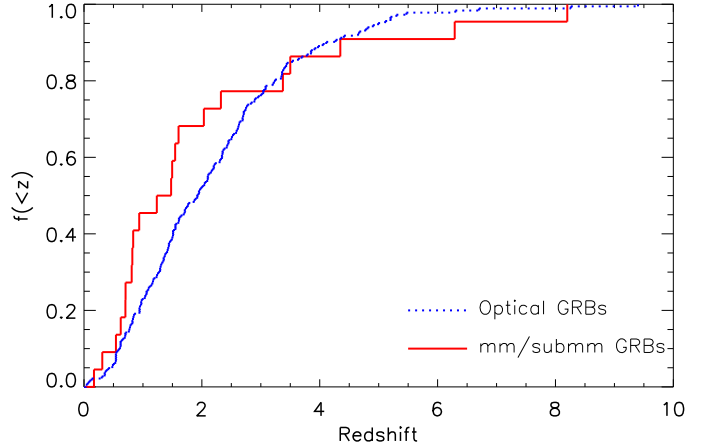


**Fig. 7.** The cumulative fraction of GRBs as a function of redshift for the optical sample of *Swift* GRBs (dotted curve; Jakobsson et al. 2012) and mm/submm-detected bursts (solid curve).

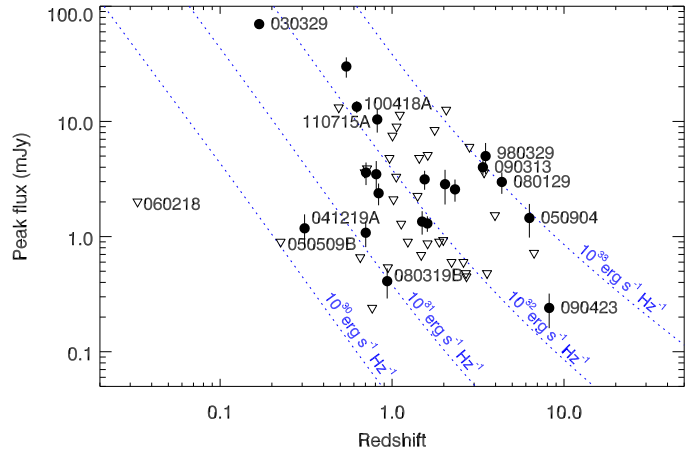


**Fig. 8.** Peak flux density measured in mm/submm (as in Fig. 4) vs. redshift. Filled dots indicate detections whereas empty triangles are detection limits. The dotted lines indicate the flux density levels for equal luminosity objects at varying redshifts. Some interesting bursts are indicated in the figure.

extreme optical brightness (Racusin et al. 2008; Bloom et al. 2009; Pandey et al. 2009) is found in the faint end of the distribution, indicating that most of the emission was concentrated in the optical bands.

On the upper part of the diagram, we identify a family of very luminous events, peaking at  $\sim 10^{33}$  erg s $^{-1}$  Hz $^{-1}$ , composed by GRB 980329 (Smith et al. 1999; Jaunsen et al. 2003), GRB 050904 (Tagliaferri et al. 2005; Haislip et al. 2006), GRB 080129 (Greiner et al. 2009) and GRB 090313 (Melandri et al. 2010), all beyond redshift 3. If those bursts were to be found at redshift of  $\sim 1$  they would reach peak fluxes of 40 mJy and easily over 100 mJy at redshifts of  $\sim 0.5$ .

On the fainter side, GRB 060218 ( $z = 0.03$ ) is the burst for which we would have the most constraining peak luminosity limits. However, this burst is known to be peculiar, being its optical emission dominated by a supernova component and not the afterglow (Campana et al. 2006; Soderberg et al. 2006; see also Thöne et al. 2011). GRB 050509B an extremely faint short burst, most probably hosted by a giant elliptical galaxy at  $z = 0.22$  (Hjorth et al. 2005; Gehrels et al. 2005; Castro-Tirado et al. 2005) is the following dimmest limit. The least luminous burst with detection in the mm/submm range is GRB 041219A,

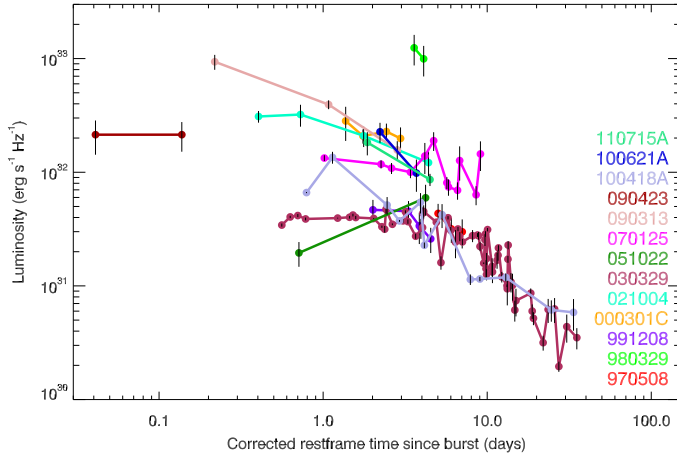


**Fig. 9.** Afterglow light curves transformed to the rest frame of the central engine. The data points of the different bands have been shifted using an offset based on the fireball model, as explained in the text.

which curiously was one of the longest and brightest GRBs detected, for which a redshift of  $z = 0.31$  has been recently suggested (Götz et al. 2011).

In the figure we also identify GRB 100418A and GRB 110715A, whose counterparts were discovered with our programmes. They are the 3rd and 4th brightest bursts ever detected in the mm/submm bands.

Using all the detections, we obtain an average peak spectral luminosity of  $10^{(32.1 \pm 0.7)} \text{ erg s}^{-1} \text{ Hz}^{-1}$ . This is roughly an order of magnitude brighter than the value found by Chandra & Frail (2012) in cm wavelengths, as expected by afterglow models. However, we note that these values must be used with care, as both samples strongly biased due to a low detection rate (25% in our case and 30% in the case of the cm range study).

Finally, we collect the light curves of GRBs with at least 2 detections and a well determined redshift, and transform them to the rest frame of the central engine to compare them directly. In Fig. 9 we plot the light curves (only detections) in luminosity and corrected of cosmological time dilation. To be able to use all the bands together, we introduce a temporal offset assuming that the light curves are described by a fireball model in which the peak frequency is evolving with  $t^{-3/2}$  (see Sect. 3.1). This is a simplistic approach but enough for a qualitative view. The intrinsic light curves appear much more clustered than the observed ones in Fig. 3 where the dispersion in fluxes was mostly due to redshift: The brightest light curve was from GRB 030329, the nearest burst and the faintest from GRB 090423, the furthest one, whereas in Fig. 9 they are both normal luminosity bursts. On the other hand, the light curves appear to be reasonably well described by the expectations of the theory described in Sect. 3.1, reaching a maximum between a few hours and a few days and then decaying.

### 3.3. Estimation of the peak flux density distribution

We can try to make a rough estimate of the distribution of peak flux densities using the data from our sample and information extrapolated from other spectral ranges. We assume that the peak flux density of GRB afterglows can be described by a Gaussian function in the logarithmic space as is seen for the flux density at specific times in other wavelengths. This Gaussian can be normalised using the fact that in band 3 we are detecting 30% of the afterglows down to a limit of  $\sim 0.9 \text{ mJy}$ . The largest uncertainty

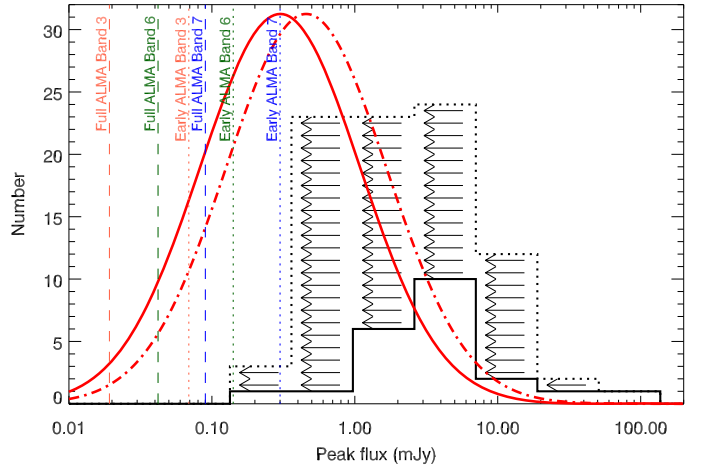


**Fig. 10.** Histogram showing the detections and detection limits of all the bands combined and an estimate of the real peak flux density distribution (indicated with a thick trace), compared to the detection limits of ALMA (from Table 5). The dashed-dotted Gaussian is the distribution derived from our sample, before correcting for the selection bias, as explained in the text.

here comes from the dispersion of the Gaussian. Using the complete catalogue of data from Kann et al. (2010) we find that the dispersion in the brightness of observed optical *R*-band magnitudes, corrected of extinction, at a specific time (1.0 days) is of 0.49, whereas for the X-rays, using the data from the burst analyser (Evans et al. 2010) find a dispersion of 0.56. Both values are quite similar, however, as the X-ray constitutes a more complete sample we will use this estimate. We must also consider that the sample of mm/submm follow-up mainly includes brighter bursts. If we calculate the average X-ray flux densities at one day of all the GRBs in the *Swift* sample and compare it with the subsample of the ones that were followed in mm/submm we find that the one first is dimmer by a factor of 1.7, which we apply to the average of the estimated distribution in mm/submm. Figure 10 shows a histogram with the detections and detection limits of all bands combined, together with the distribution of peak fluxes that has been estimated here, with an average of  $0.3 \text{ mJy}$ . Using these values we estimate that ALMA should be able to detect, using band 3, 87% of all the afterglows already in its early configuration with 16 antennas, and 98% in its full setup of 66. Using band 6, the values would be 72% (early) and 94% (full), and in band 7, 50% (early) and 82% (full).

### 3.4. Comparison with X-ray flux densities

Thanks to the X-Ray Telescope (XRT; Burrows et al. 2005) onboard *Swift*, nowadays we have early X-ray detections of the vast majority of GRB afterglows within the first minutes after the burst. These observations give us not only a precise position of the afterglow, but also a spectrum from which we can derive the unextinguished flux density, the spectral slope and the extinction due to metals in the line of sight. All this information can be used to estimate the expected flux in other wavelengths on a case to case basis assuming a synchrotron model as described in Sect. 3.1.

In this section we make a general comparison of the flux densities measured in the X-ray and mm/submm bands for those bursts that were observed by *Swift*. For the X-rays, we use the flux densities measured 0.5 days after the burst (when we can assume that the emission is dominated by the afterglow) at  $10 \text{ keV}$

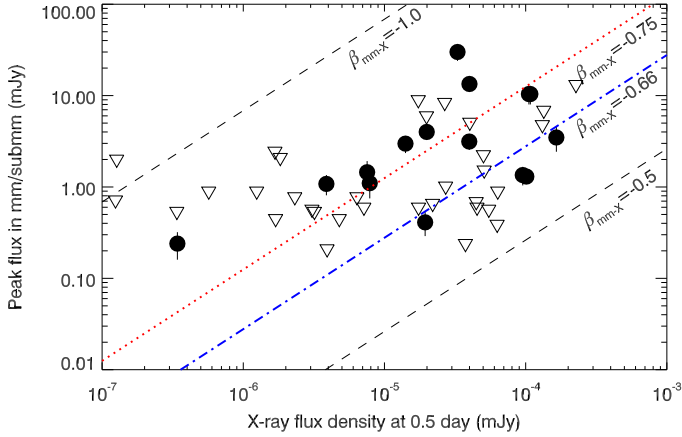


**Fig. 11.** Comparison of the peak flux density measured in mm/submm with the X-ray flux density 0.5 days after the burst (at 10 keV). Filled dots indicate detections, whereas empty triangles are  $3\sigma$  detection limits. Dashed lines indicate some characteristic slopes of the fireball model. The dotted line is the average observed in the sample of detections and the dashed-dotted line is an estimation of the real average.

(Evans et al. 2010). The scarce and heterogenous mm/submm coverage does not allow us to obtain a sample of flux densities at a given epoch. In consequence, we use, as an approximation the peak flux densities, as explained in Sect. 3. The two quantities are plotted in Fig. 11, where we can see, as expected, a correlation between the flux density measured in X-rays and in mm/submm, although with a significant dispersion.

Evans et al. (2009) found that the typical spectral slope measured in X-rays was, on average  $\beta_X \sim -1.0$  (where  $F_\nu \propto \nu^\beta$ ), which would be the slope expected for an electron index of  $p = 2.0$  if X-rays were above the cooling break ( $\nu_c$ ). The extrapolation of the X-ray measurement to mm/submm using this slope would give us the maximum flux that we could expect to measure for a synchrotron spectrum and is indicated in the figure by the upper dashed line. As expected, there is no GRB that has been measured above this extrapolation. On the other side, if  $\nu_c$  was just below X-rays, the lowest extrapolated flux would be obtained using a spectral index of  $\beta = -0.5$ , also indicated in the figure. This is what Jakobsson et al. (2004) used to define the limit for dark bursts (see Sect. 4.1). In the case of mm/submm, due to the lack of extinction or due to dust or high redshift, we would only expect to find below this threshold those bursts where  $\nu_m$  would be above the mm/submm range. In Fig. 11 we can see that all our detected bursts are located between these two limits, and mostly clustered around  $\beta = -0.75$ . On the other hand, the average flux density derived from X-rays 0.5 days after the burst (derived in a similar way as we did for 1 day in Sect. 3.3) at 10 keV is  $1.04 \times 10^{-5}$  mJy, whereas we estimated at typical peak flux density of 0.3 mJy. This would imply a typical  $\beta_{\text{mm-X}} = 0.65$ , slightly lower than the typical value for detected bursts, as expected due to the abundant detection limits.

#### 4. GRBs in the ALMA era

As shown in Figs. 3 and 4, until now the mm/submm observations of GRBs have been limited by the low sensitivity of the observations in this range as compared to other wavelengths. This is changing with the start of operations of the ALMA observatory. Even in its early configuration, ALMA will outperform the sensitivity of all previous observatories. Table 5 shows a comparison of the sensitivities (assuming equal observing conditions) of

some of the current mm/submm observatories with ALMA, both in its early and final configuration. In its final setup, the sensitivities will improve between 1 and 2 orders of magnitude. If we consider that the atmospheric conditions at the ALMA site are commonly better than the average of other observatories, the difference will be even more significant.

However, it will not only be the sensitivity, but also the spatial resolution that will allow ALMA to make breakthroughs in GRB studies. In its extended configuration, ALMA in its full array capabilities will allow resolutions of  $0.050''$  in band 3 or  $0.013''$  in band 7 ( $4.8''$  and  $1.7''$ , respectively, in the most compact configuration), allowing precise localisation of the afterglows and detailed studies of the host galaxies.

The observation of GRB 110715A that we present here, obtained during the commissioning phase of ALMA, is an advance of what this observatory will be capable of. Already the commissioning phase it was proved that ALMA can reliably perform ToO observations. Furthermore, with only 25 minutes on target, it obtained the deepest observation of a GRB in the 345 GHz band to date and allowed us to derive the most precise coordinates that are available for this afterglow.

#### 4.1. GRB afterglows

ALMA observations will play a significant role in understanding the physics of GRBs and their environment. The increased sensitivity will allow us to probe almost complete samples of afterglows, not just limited to the brightest events as we do now, eliminating most of the observational biases. In the case of very bright events ALMA will allow us to attempt, for the first time, studies of absorption spectral features, from which we will be able to derive the molecular content of distant galaxies and the chemical enrichment of the interstellar medium along the history of the Universe.

Thanks to its large collecting area, ALMA will also be able to provide polarimetric measurements for a sample or relatively bright events. As shown by Toma et al. (2008), this can give a unique view on some fundamental physics of shockwaves (though ALMA polarimetric calibration is unlikely to get better than  $\sim 1$  percent). Furthermore, simple linear polarisation measurements in submm and optical, will tell us about the plasma properties in the forward shock and the geometry of the ejecta.

One of the key areas where ALMA will play an important role will be the study of dark bursts, which strongly bias the optically selected samples of GRBs (see for example Fynbo et al. 2009). Dark bursts are those that are less luminous in the optical than what we would expect them to be assuming a synchrotron spectrum as the one explained in Sect. 3.1 based on the extrapolation of X-ray observations. Jakobsson et al. (2004) define them assuming that the electron index is  $p \geq 2$  (Sari et al. 1998), and that  $\nu_m$  is below optical frequencies (as is normally the case). Under this assumption, we would never expect a synchrotron spectrum with a slope between optical and X-rays  $\beta_{\text{OX}} > -0.5$  (note that in this paper we use the convention  $F_\nu \propto \nu^\beta$  as in Sari et al. 1998,  $\beta$  having opposite sign to the one used by Jakobsson et al. 2004). This definition was extended by van der Horst et al. (2009) not limiting the value of  $p$  and, instead, requiring  $\beta_{\text{OX}} > \beta_X + 0.5$  (being  $\beta_X$  the spectral slope measured in X-rays), given that the X-ray spectral slope is normally well constrained. This reduced optical emission can be due to optical extinction by dust, a high-redshift event (where the Lyman break is beyond the optical, at  $z \geq 5$ ) or a deviation from the simple synchrotron spectrum (like an additional inverse Compton component or a distribution of the emitting electrons

**Table 5.** Continuum flux density sensitivity ( $1\sigma$ ) with 1 h on-source observations.

Obs./Inst.	Band 3 (mJy)	Band 6 (mJy)	Band 7 (mJy)	Band 9 (mJy)
APEX (LABOCA/SABOCA) <sup>1,2</sup>	–	–	2.6	22.2
SMA <sup>3</sup>	–	0.8	2.0	29
IRAM30 m (MAMBO) <sup>4</sup>	–	0.76	–	–
PdBI (WIDEX) <sup>5</sup>	0.08	0.18	–	–
JCMT (SCUBA2) <sup>6</sup>	–	–	0.9	3.6
CARMA <sup>7</sup>	0.43	0.68	–	–
ALMA (Early) <sup>8</sup>	$2.3 \times 10^{-2}$	$4.7 \times 10^{-2}$	0.10	0.72
ALMA (Full) <sup>8</sup>	$6.4 \times 10^{-3}$	$1.4 \times 10^{-2}$	$3.0 \times 10^{-2}$	0.20

**Notes.** Based on the exposure time calculators of the different observatories operating in the mm/submm range. We assumed a precipitable water vapour of 1 mm and an average elevation of the source of 60 deg. <sup>(1)</sup> <http://www.apex-telescope.org/bolometer/laboca/obscalculator/>; <sup>(2)</sup> <http://www.apex-telescope.org/bolometer/saboca/obscalculator/>; <sup>(3)</sup> <http://sma1.sma.hawaii.edu/beamcalc.html>; <sup>(4)</sup> [https://mrt-1x3.iram.es/nite/time\\_estimator.psp#mambo](https://mrt-1x3.iram.es/nite/time_estimator.psp#mambo); <sup>(5)</sup> <http://www.iram.fr/IRAMFR/GILDAS/>; <sup>(6)</sup> [http://www.jach.hawaii.edu/JCMT/continuum/scuba2\\_integration\\_time\\_calc.html](http://www.jach.hawaii.edu/JCMT/continuum/scuba2_integration_time_calc.html); <sup>(7)</sup> <http://bima.astro.umd.edu/carma/observing/tools/rms.html>; <sup>(8)</sup> <http://www.eso.org/sci/facilities/alma/observing/tools/etc/>.

not described by a single power law). Below we give an example of each of the two main families of dark bursts.

Optically selected samples of GRBs are limited by the amount of extinction in the host galaxy that, if large, can attenuate the optical emission and make it undetectable. Hence, there is a strong bias against high extinction bursts, which limits our capability to study the star forming regions where GRBs are produced. However, the negligible effect of dust extinction in the mm/submm range allows us to detect afterglows independently of this effect, and consequently study a more complete sample. As an example of highly extinguished burst, we can look at the case of GRB 051022, with  $\beta_{\text{OX}} > 0.05$  (Castro-Tirado et al. 2007; Rol et al. 2007) one of the darkest bursts detected to date, for which an optical counterpart was not found. Precise location was obtained thanks to mm observations (Cameron & Frail 2005; Bremer et al. 2005; Castro-Tirado et al. 2007), which allowed identification of the host galaxy, for which a redshift of  $z = 0.8$  was derived (Castro-Tirado et al. 2007). A broadband study allows us to impose a lower limit on the host galaxy extinction of  $A_V > 15$  (see Fig. 12, and for other estimates also Castro-Tirado et al. 2007; Rol et al. 2007), far beyond what is typically seen in optically selected GRB afterglows.

The other main cause for optically dark GRBs is a high redshift. In these cases the absorption produced at frequencies higher than the Lyman limit does not allow us to obtain optical detections (in *R*-band) of GRB afterglows beyond redshifts of 6. These events are important to understand the formation of the first stars in the Universe. Proof that they can be detected in the mm/submm range is the fact that already in the pre-ALMA era, out of the three GRB afterglows observed at  $z > 6$ , two have been detected (GRB 050904 at  $z = 6.3$  and GRB 090423 at  $z = 8.2$ ). In Fig. 13 we have drawn the SED of GRB 050904 at  $z = 6.3$ , including radio limits (Frail et al. 2006), a detection in band 3 (and a limit in band 6) from Plateau de Bure Interferometer (Castro-Tirado et al., in prep.), near-infrared and optical data (Tagliaferri et al. 2005; Haislip et al. 2006) and X-ray data from *Swift*. In spite of its high redshift, this burst was detected with a peak flux density of 1.47 mJy in band 3, 80 times above ALMA's detection threshold for 1 h of observations in band 3. In the case of bright events it has been suggested that the study of the HD deuterium-molecule rotational-transition in absorption at  $112 \mu\text{m}$  could give us important clues on the formation of population III stars at very high redshift (Inoue et al. 2007). CO absorption lines, which

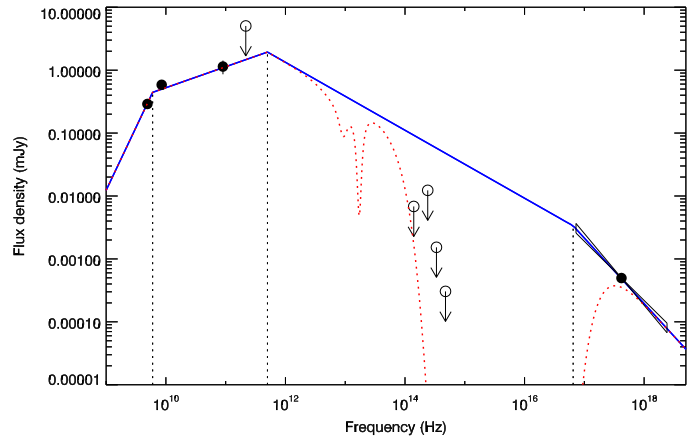


**Fig. 12.** SED of the afterglow of the dark GRB 051022. Filled dots mark detections while empty dots and arrow mark detection limits. In blue we draw a synchrotron spectrum that can explain the radio and X-ray emission, while the optical/nIR data ( $10^{14-15}$  Hz) lie well below. Adding a Small Magellanic Cloud (SMC) extinction of  $A_V \sim 15$  results in a SED (red dotted line) consistent with all the data (data obtained from Cameron & Frail 2005; Bremer et al. 2005; Castro-Tirado et al. 2007).

have been already reported through optical spectroscopy of the afterglow of GRB 080607 (Prochaska et al. 2009; Sheffer et al. 2009) are also good candidates to produce absorption features in the mm/submm range.

#### 4.2. GRB host galaxies with ALMA

Up to now the majority of GRB hosts has not been detected at mm/submm wavelengths (Tanvir et al. 2004; Berger et al. 2003; Priddey et al. 2006; Watson et al. 2011) even when dark GRBs (which are supposed to be dusty) were targeted (Barnard et al. 2003). This was interpreted as an indication that they are not heavily dust-obscured. Except for the host of the local GRB 980425 (Michałowski et al., in prep.), only three  $z \sim 1$  GRB hosts (GRB 000210, GRB 000418 and GRB 010222) were detected at mm and submm wavelengths (Frail et al. 2002; Berger et al. 2003; Tanvir et al. 2004). Their derived dust masses of a few times  $10^8 M_{\odot}$  (Michałowski et al. 2008) are comparable to that of  $z \sim 2-3$  dusty starbursts known as submm galaxies (Kovács et al. 2006; Michałowski et al. 2010). Despite these

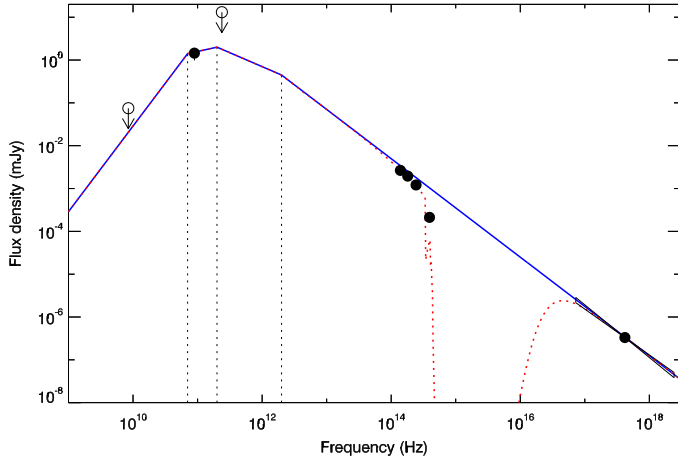


**Fig. 13.** SED of GRB 050904 at redshift  $z = 6.29$  (Kawai et al. 2006) using the detection from PdBI 5.896 days after the burst (Castro-Tirado et al., in prep.). The X-ray flux is estimated from the XRT light curve, the radio data are from Frail et al. (2006), while optical/NIR are extrapolations from Tagliaferri et al. (2005); Haislip et al. (2006). For the rough synchrotron spectrum drawn in blue, we have assumed an electron energy distribution index of  $p = 2.30$ , while an SMC extinction with  $A_V = 0.12$  (consistent with the value derived by Stratta et al. 2011; but see also Zafar et al. 2010) and Lyman blanketing (Madau 1995) have been considered in the red dotted line to match the optical/NIR observations. With these data we can constrain the position of  $\nu_a < 2 \times 10^{11}$  Hz and  $2 \times 10^{11} < \nu_c < 10^{13}$  Hz.

significant amounts of dust, these GRB hosts exhibit properties consistent with the rest of the GRB host population, namely blue optical colours, low extinction and low optical star formation rates (Gorosabel et al. 2003a,b; Galama et al. 2003; Berger et al. 2003; Savaglio et al. 2003, 2009; Christensen et al. 2004; Castro Cerón et al. 2006, 2010; Kann et al. 2006). This discrepancy was explained by Michałowski et al. (2008) by invoking very young stellar population with optical emission completely extinguished by dust. This indicates that it is virtually impossible to predict the dust emission of GRB hosts based on their optical properties and advocates for the use of ALMA to target a significant and unbiased sample of these galaxies.

Despite numerous attempts, CO emission has not been detected for any GRB host galaxy (Kohno et al. 2005; Endo et al. 2007; Hatsukade et al. 2007, 2011; Stanway et al. 2011); we refer to Table 1 in Hatsukade et al. (2011) for a homogeneous overview of all available limits on CO line luminosities of GRB hosts. The derived upper limits on molecular gas masses of  $10^8$ – $10^9 M_\odot$  indicate that GRB hosts are not as gas-rich as submm galaxies (Greve et al. 2005; Ivison et al. 2011).

We further note that the recent discovery of strong CO and  $H_2$  features in absorption in an optical spectrum of the afterglow of GRB 080607 (Prochaska et al. 2009; Sheffer et al. 2009) highlights the value of ALMA molecular line observations in tandem with optical spectroscopy. The detection of vibrationally excited transitions ( $H_2^+$ ) in the afterglow of GRB 080607 (Sheffer et al. 2009), likely excited by the UV flux of the afterglow, show the importance of repeated spectroscopic observations by ALMA to probe the ISM properties of the host galaxies through time variable lines.

The unprecedented sensitivity of ALMA in the mm and submm wavelengths, will allow the study of GRB host galaxies through both continuum and emission line observations. ALMA is sensitive enough to probe the dust properties of representative GRB hosts, not only the most star-forming ones. Moreover,

the excellent angular resolution of ALMA will allow spatially-resolved studies of these galaxies. This is important as there are indications that the immediate environments (1–3 kpc) of GRBs are the most star-forming sites within their host galaxies (Bloom et al. 2002; Fruchter et al. 2006; Thöne et al. 2008; Östlin et al. 2008; Michałowski et al. 2009).

To date, measured spectroscopic GRB redshifts range between 0.0085 and 8.2. Figure 14 shows a number of spectral features that will be covered by the different ALMA bands for a range of redshifts between  $z = 0$  up to  $z = 10$ . Taking into account the weather constraints at the highest bands, we consider that bands 3 to 7 will be better suited for host detections. For the nearer events ( $z \lesssim 4$ ) the carbon monoxide ladder of rotational transitions up to  $J = 11$ –10 could be feasible as reported for the submillimeter galaxy SMM J16359+6612 (at  $z = 2.52$ ; Weiß et al. 2005b) and the broad absorption line quasar APM08279+5255 (at  $z = 3.87$ ; Weiß et al. 2007). Additionally, the fine structure transitions of neutral carbon at 492 and 809 GHz were also detected towards APM08279+5255 (Weiß et al. 2005a; Wagg et al. 2006). Moreover, [CI] at 809 GHz and CO  $J = 7$ –6, separated  $\sim 2.4$  GHz in the rest frame, could be observed simultaneously for redshifts of  $z \sim 2$ –8 provided the large bandwidth of ALMA receivers. At redshifts above  $z = 4$ –5, the higher- $J$  CO transitions will still be visible mostly within bands 3 to 5. Above that redshift, the fine structure lines of the most abundant elements, O, C, and N, will be the best suited ISM tracers. In particular the fine structure line of [CII] at  $158 \mu\text{m}$  is likely the brightest emission line observable at high- $z$  (Maiolino et al. 2009). The lines of [OIII] at  $52 \mu\text{m}$  and  $88 \mu\text{m}$  and [OI] at  $63 \mu\text{m}$  have also been reported towards high-redshift lensed systems (Ferkinhoff et al. 2010; Sturm et al. 2010).

## 5. Conclusions

This paper presents the most complete catalogue of GRB observations in the mm/submm range to date, including observations of 11 GRBs from our programmes at APEX and SMA. We include a short observation of a GRB obtained with the ALMA observatory during its commissioning phase and with only 7 antennas, that gives an early idea of the potential of the observatory. The total sample contains data from 102 GRBs. Among this collection of observations, there are 88 observations of GRB afterglows, of which 22 (25%) were detected (two of them discovered within our programmes) and 35 of host galaxies, of which 4 were detected. Observations until now have been strongly limited by the sensitivity of the instruments in this range, imposing important biases to any statistical study performed with them. Even with these limitations, we have proved that it is already possible to detect counterparts to GRBs in the mm/submm range with redshifts ranging from 0.168 all the way up to 8.2. This spectral range has also proved to be a very useful tool to localise and characterise the counterparts of dark GRBs, which are elusive in optical wavelengths.

Within the sample bursts have peak luminosities spanning over 2.5 orders of magnitude, with the most luminous reaching  $10^{33} \text{ erg s}^{-1} \text{ Hz}^{-1}$ . If such a burst happened at redshift of  $\sim 1$  they would reach peak fluxes of 40 mJy and over 100 mJy at redshifts of  $\sim 0.5$ . Comparing with X-rays, we find a correlation of the peak flux density in mm/submm with the X-ray flux density at 0.5 days that can serve to make rough predictions of mm/submm brightness from the early X-ray data. Using data from the sample and assumptions based on samples at other wavelengths, an estimate of the real peak flux density distribution of GRBs is made,

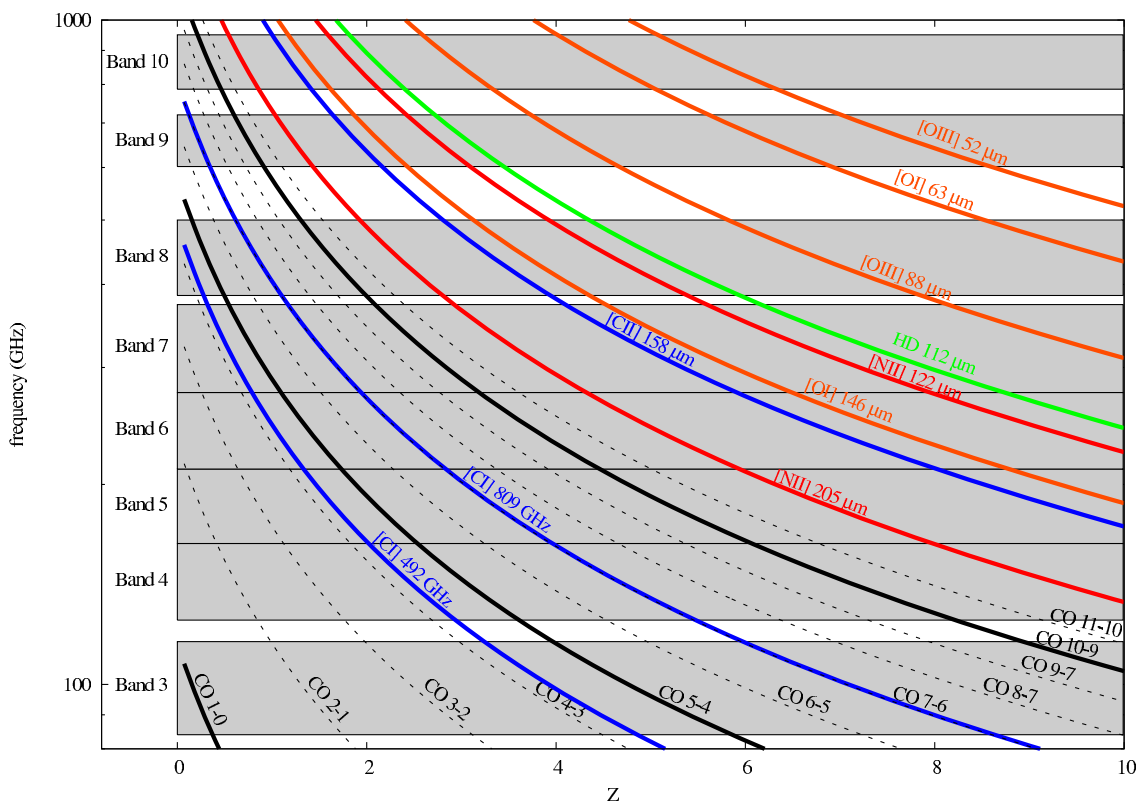


**Fig. 14.** Spectral lines observable at each ALMA band as a function of the redshift. Different colours have been used to indicate different elements.

from which an average peak flux density value of 0.33 mJy can be expected.

On the 30th September 2011, the ALMA observatory started scientific operations with a limited setup of 16 antennas. Already then, it became the most sensitive observatory in the mm/submm range, increasing the sensitivity and resolution by around an order of magnitude with respect to the previous instrumentation, being even more significant in the highest frequencies. The final full observatory, with 66 antennas will set completely new standards in the field. In addition to the improved sensitivity and resolution, ALMA will be capable of observing in a very wide range of frequencies, that was never covered before by a single observatory. Using our peak flux density estimates and the detection limits calculated for ALMA, we can expect that early ALMA will detect around 87% of the bursts, while full ALMA should be able to detect 98%. In the case of bright GRB afterglows, like GRB 030329, GRB 100621A, GRB 100418A or GRB 110715A, where fluxes reached tens of mJy, ALMA will be able to study spectral features and perform polarimetric studies of the afterglow, which have been out of reach until now.

With ALMA we will be, for the first time, in position to undertake studies of samples of GRB host galaxies. We will be able to perform studies of the continuum emission to characterise the dust content and determine the unextinguished star formation rate of the hosts. Through the study of emission features from the host, we will be able to understand the molecular content and the chemical enrichment of the strong star-forming regions in which GRBs are found, at redshifts that go back to the epoch in which the first stars were formed.

*Acknowledgements.* A.d.U.P. acknowledges support from ESO's Scientific Visitor Programme in Chile, where a significant part of this work was done. The Dark Cosmology Centre is funded by the Danish National Research Foundation. The Atacama Large Millimeter/submillimeter Array (ALMA), an international astronomy facility, is a partnership of Europe, North America and East Asia in

cooperation with the Republic of Chile. This paper makes use of the following ALMA Science Verification data: ADS/JAO.ALMA#2011.0.00006.SV. We are grateful for the support from the ALMA commissioning team. APEX is a collaboration between the Max-Planck-Institut für Radioastronomie, the European Southern Observatory, and the Onsala Space Observatory. The Submillimeter Array is a joint project between the Smithsonian Astrophysical Observatory and the Academia Sinica Institute of Astronomy and Astrophysics and is funded by the Smithsonian Institution and the Academia Sinica. This paper made use of observations carried out with the IRAM Plateau de Bure Interferometer. IRAM is supported by INSU/CNRS (France), MPG (Germany) and IGN (Spain). This work made use of data supplied by the UK Swift Science Data Centre at the University of Leicester. We acknowledge partial support from the Spanish Ministry of Science and Innovation through programmes AYA20082008-03467/ESP and AYA2009-14000-C03-01. S.S. acknowledges support by a Grant of Excellence from the Icelandic Research Fund.

## References

- Akerlof, C., Balsano, R., Barthelmy, S., et al. 1999, *Nature*, 398, 400
- Antonelli, L. A., Maund, J. R., Palazzi, E., et al. 2010, *GRB Coordinates Network*, 10620
- Barnard, V. E., Blain, A. W., Tanvir, N. R., et al. 2003, *MNRAS*, 338, 1
- Barnard, V., Schieven, G., Tilanus, R., Lundin, E., & Ivison, R. 2005, *GRB Coordinates Network*, 3515
- Barthelmy, S. D., Burrows, D. N., Cummings, J. R., et al. 2011, *GRB Coordinates Network*, 12124
- Berger, E., Sari, R., Frail, D. A., et al. 2000, *ApJ*, 545, 56
- Berger, E., Cowie, L. L., Kulkarni, S. R., et al. 2003, *ApJ*, 588, 99
- Bertoldi, F., Frail, D. A., Weiss, A., et al. 2002, *GRB Coordinates Network*, 1497
- Bertoldi, F., Bonn, M., Frail, D. A., et al. 2003a, *GRB Coordinates Network*, 2440
- Bertoldi, F., Frail, D. A., Berger, E., Menten, K. M., & Kulkarni, S. 2003b, *GRB Coordinates Network*, 1835
- Bertoldi, F., Frail, D. A., Weiss, A., et al. 2005, *GRB Coordinates Network*, 3091
- Björnsson, G., Gudmundsson, E. H., & Jóhannesson, G. 2004, *ApJ*, 615, L77
- Blake, C. H., Bloom, J. S., Starr, D. L., et al. 2005, *Nature*, 435, 181
- Bloom, J. S., Kulkarni, S. R., & Djorgovski, S. G. 2002, *AJ*, 123, 1111
- Bloom, J. S., Perley, D. A., Li, W., et al. 2009, *ApJ*, 691, 723
- Bock, D., Chandra, P., Frail, D. A., & Kulkarni, S. R. 2009a, *GRB Coordinates Network*, 9005

- Bock, D., Chandra, P., Frail, D. A., & Kulkarni, S. R. 2009b, GRB Coordinates Network, 9274
- Bremer, M., & Castro-Tirado, A. J. 2002, GRB Coordinates Network, 1487
- Bremer, M., Krichbaum, T. P., Galama, T. J., et al. 1998, A&A, 332, L13
- Bremer, M., Castro-Tirado, A. J., & Neri, R. 2005, GRB Coordinates Network, 4157
- Burrows, D. N., Hill, J. E., Nousek, J. A., et al. 2005, Space Sci. Rev., 120, 165
- Cameron, P. B., & Frail, D. A. 2005, GRB Coordinates Network, 4154
- Campana, S., Mangano, V., Blustin, A. J., et al. 2006, Nature, 442, 1008
- Castro Cerón, J. M., Gorosabel, J., Castro-Tirado, A. J., et al. 2004, A&A, 424, 833
- Castro Cerón, J. M., Michałowski, M. J., Hjorth, J., et al. 2006, ApJ, 653, L85
- Castro Cerón, J. M., Michałowski, M. J., Hjorth, J., et al. 2010, ApJ, 721, 1919
- Castro-Tirado, A. J., de Ugarte Postigo, A., Gorosabel, J., et al. 2005, A&A, 439, L15
- Castro-Tirado, A. J., Bremer, M., McBreen, S., et al. 2007, A&A, 475, 101
- Castro-Tirado, A. J., Bremer, M., Winters, J., et al. 2009a, GRB Coordinates Network, 9100
- Castro-Tirado, A. J., Bremer, M., Winters, J., et al. 2009b, GRB Coordinates Network, 9273
- Cenko, S. B., Frail, D. A., Harrison, F. A., et al. 2010, ApJ, 711, 641
- Chandra, P., & Frail, D. A. 2010, GRB Coordinates Network, Circular Service, 11257, 1, 1257
- Chandra, P., & Frail, D. A. 2012, ApJ, in press [arXiv:1110.4124]
- Chandra, P., Cenko, S. B., Frail, D. A., et al. 2008, ApJ, 683, 924
- Chandra, P., Frail, D. A., Fox, D., et al. 2010, ApJ, 712, L31
- Chattopadhyay, T., Misra, R., Chattopadhyay, A. K., & Naskar, M. 2007, ApJ, 667, 1017
- Chormock, R., Berger, E., Fox, D., et al. 2010, GRB Coordinates Network, Circular Service, 11164, 1
- Christensen, L., Hjorth, J., & Gorosabel, J. 2004, A&A, 425, 913
- Costa, E., Frontera, F., Heise, J., et al. 1997, Nature, 387, 783
- Covino, S., Campana, S., Conciatore, M. L., et al. 2010, A&A, 521, A53
- Dai, Z. G., & Lu, T. 1998, A&A, 333, L87
- Dai, Z. G., & Lu, T. 2002, ApJ, 565, L87
- de Ugarte Postigo, A., Castro-Tirado, A. J., Gorosabel, J., et al. 2005, A&A, 443, 841
- de Ugarte Postigo, A., Fatkhullin, T. A., Jóhannesson, G., et al. 2007, A&A, 462, L57
- de Ugarte Postigo, A., Lundgren, A., De Breuck, C., Castro-Tirado, A. J., & Jelinek, M. 2009a, GRB Coordinates Network, 10129
- de Ugarte Postigo, A., Lundgren, A., De Breuck, C., et al. 2009b, GRB Coordinates Network, 10206
- de Ugarte Postigo, A., De Breuck, C., Castro-Tirado, A. J., et al. 2010a, GRB Coordinates Network, 11098
- de Ugarte Postigo, A., Flores, H., Wiersema, K., et al. 2010b, GRB Coordinates Network, 11307
- de Ugarte Postigo, A., Goldoni, P., Thöne, C. C., et al. 2010c, A&A, 513, A42
- de Ugarte Postigo, A., Lundgren, A., Wyrowski, F., et al. 2010d, GRB Coordinates Network, 11304
- de Ugarte Postigo, A., Martín-Ruiz, S., Petitpas, G., & Castro-Tirado, A. J. 2010e, GRB Coordinates Network, 11211
- de Ugarte Postigo, A., Castro-Tirado, A. J., & Gorosabel, J. 2011a, GRB Coordinates Network, Circular Service, 11978, 1
- de Ugarte Postigo, A., Castro-Tirado, A. J., Tello, J. C., Cabrera Lavers, A., & Reverte, D. 2011b, GRB Coordinates Network, Circular Service, 11993
- de Ugarte Postigo, A., De Breuck, C., Lundgren, A., & Dumke, M. 2011c, GRB Coordinates Network, 12381
- de Ugarte Postigo, A., Lundgren, A., De Breuck, C., et al. 2011d, GRB Coordinates Network, 12151
- de Ugarte Postigo, A., Lundgren, A., Mac-Auliffe, F., et al. 2011e, GRB Coordinates Network, 12168
- de Ugarte Postigo, A., Petitpas, G., & Martin, S. 2011f, GRB Coordinates Network, 12002
- Endo, A., Kohno, K., Hatsukade, B., et al. 2007, ApJ, 659, 1431
- Esin, A. A., & Blandford, R. 2000, ApJ, 534, L151
- Evans, P. A., Beardmore, A. P., Page, K. L., et al. 2009, MNRAS, 397, 1177
- Evans, P. A., Willingale, R., Osborne, J. P., et al. 2010, A&A, 519, A102
- Ferkinhoff, C., Hailey-Dunsheath, S., Nikola, T., et al. 2010, ApJ, 714, L147
- Fong, W., & Berger, E. 2011, GRB Coordinates Network, 12155
- Frail, D. A., Kulkarni, S. R., Nicastro, L., Feroci, M., & Taylor, G. B. 1997, Nature, 389, 261
- Frail, D. A., Berger, E., Galama, T., et al. 2000, ApJ, 538, L129
- Frail, D. A., Bertoldi, F., Moriarty-Schieven, G. H., et al. 2002, ApJ, 565, 829
- Frail, D. A., Cameron, P. B., Kasliwal, M., et al. 2006, ApJ, 646, L99
- Fruchter, A. S., Levan, A. J., Strolger, L., et al. 2006, Nature, 441, 463
- Fynbo, J. P. U., Jakobsson, P., Prochaska, J. X., et al. 2009, ApJS, 185, 526
- Galama, T. J., Briggs, M. S., Wijers, R. A. M. J., et al. 1999, Nature, 398, 394
- Galama, T. J., Bremer, M., Bertoldi, F., et al. 2000, ApJ, 541, L45
- Galama, T. J., Reichart, D., Brown, T. M., et al. 2003, ApJ, 587, 135
- Garnavich, P. M., Loeb, A., & Stanek, K. Z. 2000, ApJ, 544, L11
- Gehrels, N., Sarazin, C. L., O'Brien, P. T., et al. 2005, Nature, 437, 851
- Golenetskii, S., Aptekar, R., Frederiks, D., et al. 2011, GRB Coordinates Network, 12362
- Gorosabel, J., Christensen, L., Hjorth, J., et al. 2003a, A&A, 400, 127
- Gorosabel, J., Klose, S., Christensen, L., et al. 2003b, A&A, 409, 123
- Gorosabel, J., de Ugarte Postigo, A., Castro-Tirado, A. J., et al. 2010, A&A, 522, A14
- Götz, D., Covino, S., Hascoët, R., et al. 2011, MNRAS, 413, 2173
- Granot, J., Nakar, E., & Piran, T. 2003, Nature, 426, 138
- Greiner, J., Krühler, T., McBreen, S., et al. 2009, ApJ, 693, 1912
- Greiner, J., Peimbert, M., Estaban, C., et al. 2003, GRB Coordinates Network, 2020
- Greve, T. R., Bertoldi, F., Smail, I., et al. 2005, MNRAS, 359, 1165
- Gruendl, R. A., Smith, I. A., Forester, R., et al. 1998, in Gamma-Ray Bursts, 4th Hunstville Symposium, ed. C. A. Meegan, R. D. Preece, & T. M. Koshut, AIP Conf. Ser., 428, 576
- Güsten, R., Nyman, L. Å., Schilke, P., et al. 2006, A&A, 454, L13
- Haislip, J. B., Nysewander, M. C., Reichart, D. E., et al. 2006, Nature, 440, 181
- Hatsukade, B., Kohno, K., Endo, A., et al. 2007, PASJ, 59, 67
- Hatsukade, B., Kohno, K., Endo, A., Nakanishi, K., & Ohta, K. 2011, ApJ, 738, 33
- Hjorth, J., Sollerman, J., Møller, P., et al. 2003, Nature, 423, 847
- Hjorth, J., Sollerman, J., Gorosabel, J., et al. 2005, ApJ, 630, L117
- Huang, M., Zhang, B., Xu, D., et al. 2011, GRB Coordinates Network, 12006
- Inoue, S., Omukai, K., & Ciardi, B. 2007, MNRAS, 380, 1715
- Ioka, K., & Nakamura, T. 2001, ApJ, 561, 703
- Iverson, R. J., Papadopoulos, P. P., Smail, I., et al. 2011, MNRAS, 412, 1913
- Jakobsson, P., Hjorth, J., Fynbo, J. P. U., et al. 2004, ApJ, 617, L21
- Jakobsson, P., Hjorth, J., Malesani, D., et al. 2012, ApJ, in press
- Jaunsen, A. O., Andersen, M. I., Hjorth, J., et al. 2003, A&A, 402, 125
- Jelínek, M., Prouza, M., Kubánek, P., et al. 2006, A&A, 454, L119
- Jóhannesson, G., Björnsson, G., & Gudmundsson, E. H. 2006, ApJ, 647, 1238
- Kann, D. A., Klose, S., & Zeh, A. 2006, ApJ, 641, 993
- Kann, D. A., Klose, S., Zhang, B., et al. 2010, ApJ, 720, 1513
- Kawai, N., Kosugi, G., Aoki, K., et al. 2006, Nature, 440, 184
- King, A., Olsson, E., & Davies, M. B. 2007, MNRAS, 374, L34
- Klebesadel, R. W., Strong, I. B., & Olson, R. A. 1973, ApJ, 182, L85
- Kohno, K., Tosaki, T., Okuda, T., et al. 2005, PASJ, 57, 147
- Kovács, A. 2008, in SPIE Conf. Ser., 7020
- Kovács, A., Chapman, S. C., Dowell, C. D., et al. 2006, ApJ, 650, 592
- Kumar, P., & Piran, T. 2000, ApJ, 535, 152
- Kuno, N., Sato, N., Nakanishi, H., et al. 2004, PASJ, 56, L1
- Levan, A. J., Wynn, G. A., Chapman, R., et al. 2006, MNRAS, 368, L1
- Levan, A. J., Tanvir, N. R., Wiersema, K., Berger, E., & Fox, D. 2011, GRB Coordinates Network, 12368
- Lipkin, Y. M., Ofek, E. O., Gal-Yam, A., et al. 2004, ApJ, 606, 381
- Loeb, A., & Perna, R. 1998, ApJ, 495, 597
- Madau, P. 1995, ApJ, 441, 18
- Maiolino, R., Caselli, P., Nagao, T., et al. 2009, A&A, 500, L1
- Malesani, D., Hjorth, J., Jakobsson, P., et al. 2008, GRB Coordinates Network, 7169
- Malesani, D., Fugazza, D., D'Avanzo, P., et al. 2011, GRB Coordinates Network, Circular Service, 11977, 1
- Mangano, V., Sbarufatti, B., Evans, P. A., & Krimm, H. A. 2011, GRB Coordinates Network, 12364
- Martin, S., Petitpas, G., de Ugarte Postigo, A., et al. 2010, GRB Coordinates Network, 10630
- Melandri, A., Kobayashi, S., Mundell, C. G., et al. 2010, ApJ, 723, 1331
- Mészáros, P., & Gruzinov, A. 2000, ApJ, 543, L35
- Mészáros, P., Rees, M. J., & Wijers, R. A. M. J. 1998, ApJ, 499, 301
- Michałowski, M. J., Hjorth, J., Castro Cerón, J. M., & Watson, D. 2008, ApJ, 672, 817
- Michałowski, M. J., Hjorth, J., Malesani, D., et al. 2009, ApJ, 693, 347
- Michałowski, M., Hjorth, J., & Watson, D. 2010, A&A, 514, A67
- Morgan, A. N., & Bower, G. C. 2009, GRB Coordinates Network, 9685
- Nakar, E., & Piran, T. 2003, ApJ, 598, 400
- Narayan, R., Paczynski, B., & Piran, T. 1992, ApJ, 395, L83
- O'Meara, J., Chen, H.-W., & Prochaska, J. X. 2010, GRB Coordinates Network, Circular Service, 11089, 1, 1089
- Östlin, G., Zackrisson, E., Sollerman, J., Mattila, S., & Hayes, M. 2008, MNRAS, 387, 1227
- Paczynski, B. 1990, ApJ, 363, 218
- Paczynski, B. 1998, in Gamma-Ray Bursts, 4th Hunstville Symposium, ed. C. A. Meegan, R. D. Preece, & T. M. Koshut, AIP Conf. Ser., 428, 783
- Pandey, S. B., Sagar, R., Anupama, G. C., et al. 2004, A&A, 417, 919
- Pandey, S. B., Castro-Tirado, A. J., McBreen, S., et al. 2006, A&A, 460, 415

- Pandey, S. B., Castro-Tirado, A. J., Jelínek, M., et al. 2009, *A&A*, 504, 45
- Pérez-Ramírez, D., de Ugarte Postigo, A., Gorosabel, J., et al. 2010, *A&A*, 510, A105
- Petitpas, G., Zauderer, A., Berger, E., et al. 2011, GRB Coordinates Network, 11650
- Piran, T. 1999, *Phys. Rep.*, 314, 575
- Piranomonte, S., Vergani, S. D., Malesani, D., Fynbo, J. P. U., & Wiersema, K. 2011, GRB Coordinates Network, 12164
- Priddey, R. S., Tanvir, N. R., Levan, A. J., et al. 2006, *MNRAS*, 369, 1189
- Prochaska, J. X., Sheffer, Y., Perley, D. A., et al. 2009, *ApJ*, 691, L27
- Racusin, J. L., Karpov, S. V., Sokolowski, M., et al. 2008, *Nature*, 455, 183
- Ramirez-Ruiz, E. 2004, *MNRAS*, 349, L38
- Ramirez-Ruiz, E., Dray, L. M., Madau, P., & Tout, C. A. 2001, *MNRAS*, 327, 829
- Rees, M. J., & Meszaros, P. 1992, *MNRAS*, 258, 41
- Rees, M. J., & Meszaros, P. 1998, *ApJ*, 496, L1
- Reichart, D. E. 2001, *ApJ*, 554, 643
- Resmi, L., Ishwara-Chandra, C. H., Castro-Tirado, A. J., et al. 2005, *A&A*, 440, 477
- Rhoads, J. E. 1999, *ApJ*, 525, 737
- Riechers, D. A., Walter, F., Bertoldi, F., Carilli, C. L., & Cox, P. 2009a, GRB Coordinates Network, 9321
- Riechers, D. A., Walter, F., Bertoldi, F., et al. 2009b, GRB Coordinates Network, 9322
- Rol, E., van der Horst, A., Wiersema, K., et al. 2007, *ApJ*, 669, 1098
- Rossi, E., Lazzati, D., & Rees, M. J. 2002, *MNRAS*, 332, 945
- Rossi, A., de Ugarte Postigo, A., Ferrero, P., et al. 2008, *A&A*, 491, L29
- Sagar, R., Stalin, C. S., Bhattacharya, D., et al. 2001, *BASI*, 29, 91
- Salvaterra, R., Della Valle, M., Campana, S., et al. 2009, *Nature*, 461, 1258
- Sari, R., & Mészáros, P. 2000, *ApJ*, 535, L33
- Sari, R., Piran, T., & Narayan, R. 1998, *ApJ*, 497, L17
- Sault, R. J., Teuben, P. J., & Wright, M. C. H. 1995, in *Astronomical Data Analysis Software and Systems IV*, ed. R. A. Shaw, H. E. Payne, & J. J. E. Hayes, ASP Conf. Ser., 77, 433
- Savaglio, S., Fall, S. M., & Fiore, F. 2003, *ApJ*, 585, 638
- Savaglio, S., Glazebrook, K., & LeBorgne, D. 2009, *ApJ*, 691, 182
- Sheffer, Y., Prochaska, J. X., Draine, B. T., Perley, D. A., & Bloom, J. S. 2009, *ApJ*, 701, L63
- Shepherd, D. S., Metzger, M. R., & Kulkarni, S. R. 1997, *IAU Circ.*, 6664, 1
- Sheth, K., Frail, D. A., White, S., et al. 2003, *ApJ*, 595, L33
- Siringo, G., Kreysa, E., Kovács, A., et al. 2009, *A&A*, 497, 945
- Smith, I. A., Gruendl, R. A., Liang, E. P., & Lo, K. Y. 1997, *ApJ*, 487, L5
- Smith, I. A., Tilanus, R. P. J., van Paradijs, J., et al. 1999, *A&A*, 347, 92
- Smith, I. A., Tilanus, R. P. J., Wijers, R. A. M. J., et al. 2001, *A&A*, 380, 81
- Smith, I. A., Tilanus, R. P. J., Tanvir, N., et al. 2005a, *A&A*, 439, 987
- Smith, I. A., Tilanus, R. P. J., Tanvir, N., et al. 2005b, *A&A*, 439, 981
- Soderberg, A. M., Kulkarni, S. R., Nakar, E., et al. 2006, *Nature*, 442, 1014
- Soderberg, A. M., Berger, E., Page, K. L., et al. 2008, *Nature*, 453, 469
- Stanek, K. Z., Matheson, T., Garnavich, P. M., et al. 2003, *ApJ*, 591, L17
- Stanway, E. R., Bremer, M. N., Tanvir, N. R., Levan, A. J., & Davies, L. J. M. 2011, *MNRAS*, 410, 1496
- Stratta, G., Gallerani, S., & Maiolino, R. 2011, *A&A*, 532, A45
- Sturm, E., Verma, A., Graciá-Carpio, J., et al. 2010, *A&A*, 518, L36
- Svensson, K. M., Tanvir, N. R., Perley, D. A., et al. 2011, *MNRAS*, accepted [arXiv:1109.3167]
- Tagliaferri, G., Antonelli, L. A., Chincarini, G., et al. 2005, *A&A*, 443, L1
- Tanvir, N. R., Barnard, V. E., Blain, A. W., et al. 2004, *MNRAS*, 352, 1073
- Tanvir, N. R., Fox, D. B., Levan, A. J., et al. 2009, *Nature*, 461, 1254
- Tanvir, N. R., Wiersema, K., Levan, A. J., Greiss, S., & Gaensicke, B. 2011, GRB Coordinates Network, 12365
- Taylor, G. B., Frail, D. A., Kulkarni, S. R., et al. 1998, *ApJ*, 502, L115
- Thöne, C. C., Fynbo, J. P. U., Östlin, G., et al. 2008, *ApJ*, 676, 1151
- Thöne, C. C., de Ugarte Postigo, A., Fryer, C. L., et al. 2011, *Nature*, 480, 72
- Toma, K., Ioka, K., & Nakamura, T. 2008, *ApJ*, 673, L123
- van der Horst, A. J., Kouveliotou, C., Gehrels, N., et al. 2009, *ApJ*, 699, 1087
- van der Horst, A. J., Linford, J. D., Taylor, G. B., et al. 2010a, *The Astronomer's Telegram*, 2918, 1
- van der Horst, A. J., Wiersema, K., Kamble, A. P., et al. 2010b, GRB Coordinates Network, Circular Service, 11256, 1
- van der Horst, A. J., Wiersema, K., Kamble, A. P., et al. 2010c, GRB Coordinates Network, Circular Service, 11221, 1
- van Paradijs, J., Groot, P. J., Galama, T., et al. 1997, *Nature*, 386, 686
- Vergani, S. D., Flores, H., Covino, S., et al. 2011, *A&A*, 535, A127
- Wagg, J., Wilner, D. J., Neri, R., Downes, D., & Wiklind, T. 2006, *ApJ*, 651, 46
- Walter, F., Carilli, C., Bertoldi, F., & Weiss, A. 2006, GRB Coordinates Network, 5300
- Wang, X., & Loeb, A. 2000, *ApJ*, 535, 788
- Watson, D., French, J., Christensen, L., et al. 2011, *ApJ*, 741, 58
- Weiß, A., Downes, D., Henkel, C., & Walter, F. 2005a, *A&A*, 429, L25
- Weiß, A., Downes, D., Walter, F., & Henkel, C. 2005b, *A&A*, 440, L45
- Weiß, A., Downes, D., Neri, R., et al. 2007, *A&A*, 467, 955
- Wijers, R. A. M. J., & Galama, T. J. 1999, *ApJ*, 523, 177
- Woosley, S. E. 1993, *ApJ*, 405, 273
- Zafar, T., Watson, D. J., Malesani, D., et al. 2010, *A&A*, 515, A94
- Zauderer, A., & Berger, E. 2011, GRB Coordinates Network, 12190
- Zauderer, A., Berger, E., & Frail, D. 2011a, GRB Coordinates Network, 11661
- Zauderer, A., Frail, D. A., Berger, E., & Kulkarni, S. R. 2011b, GRB Coordinates Network, 11580
- Zauderer, A., Petitpas, G., & Berger, E. 2011c, GRB Coordinates Network, 12189
- Zhang, B., & Mészáros, P. 2002, *ApJ*, 566, 712
- Zheng, W., Shen, R. F., Sakamoto, T., et al. 2011, *ApJ*, submitted [arXiv:1111.0283]

**Table 1.** Pre-ALMA observations of GRBs in the millimeter and submillimeter range.

GRB	Redshift	Observatory	$t - t_0$ (days)	Band (GHz)	Flux density (mJy)	Reference
970111	—	BIMA	30.180	85.0	< 30.00 (0.00 ± 10.00)	Smith et al. 1997
		BIMA	33.190	85.0	< 4.20 (0.00 ± 1.40)	Smith et al. 1997
970228	0.69	BIMA	5.970	85.0	< 16.50 (0.00 ± 5.50)	Smith et al. 1997
		BIMA	6.990	86.4	< 3.60 (0.00 ± 1.20)	Smith et al. 1997
		JCMT	Late	350.0	< 3.09 (−0.76 ± 1.03)	Berger et al. 2003
		JCMT	Late	350.0	< 3.96 (1.78 ± 1.32)	Tanvir et al. 2004
		JCMT	Late	670.0	< 54.90 (−21.40 ± 18.30)	Berger et al. 2003
970508	0.83	BIMA	1.296	85.0	< 82.80 (0.00 ± 27.60)	Gruendl et al. 1998
		BIMA	2.046	85.0	< 21.60 (0.00 ± 7.20)	Gruendl et al. 1998
		OVRO	2.246	86.8	< 10.80 (0.00 ± 3.60)	Shepherd et al. 1997
		OVRO	3.266	86.8	< 7.80 (0.00 ± 2.60)	Shepherd et al. 1997
		BIMA	6.346	85.0	< 16.20 (0.00 ± 5.40)	Gruendl et al. 1998
		BIMA	7.346	85.0	< 17.10 (0.00 ± 5.70)	Gruendl et al. 1998
		BIMA	8.296	85.0	< 28.80 (0.00 ± 9.60)	Gruendl et al. 1998
		PdBI	8.516	86.2	< 2.40 (0.45 ± 0.80)	Bremer et al. 1998
		PdBI	10.170	86.2	2.38 ± 0.51	Bremer et al. 1998
		PdBI	12.241	86.2	1.74 ± 0.43	Bremer et al. 1998
		PdBI	14.086	87.8	1.64 ± 0.47	Bremer et al. 1998
		PdBI	14.471	87.8	< 1.83 (0.38 ± 0.61)	Bremer et al. 1998
		PdBI	19.506	86.0	< 0.87 (−0.01 ± 0.29)	Bremer et al. 1998
		BIMA	21.200	85.0	< 14.40 (0.00 ± 4.80)	Gruendl et al. 1998
		PdBI	Late	86.6	< 1.14 (0.14 ± 0.38)	Bremer et al. 1998
		PdBI	10.170	232.0	< 6.81 (1.62 ± 2.27)	Bremer et al. 1998
		PdBI	12.241	232.0	< 6.33 (−3.05 ± 2.11)	Bremer et al. 1998
		PdBI	14.086	228.4	< 9.00 (0.67 ± 3.00)	Bremer et al. 1998
		JCMT	18.000	220.0	< 30.00 (0.00 ± 10.00)	Smith et al. 1999
		JCMT	Late	350.0	< 3.03 (−1.57 ± 1.01)	Berger et al. 2003
JCMT	Late	670.0	< 102.00 (6.00 ± 34.00)	Berger et al. 2003		
970828	0.96	JCMT	Late	350.0	< 7.08 (1.26 ± 2.36)	Barnard et al. 2003
971214	3.43	JCMT	1.560	350.0	< 9.00 (0.00 ± 3.00)	Smith et al. 1999
		JCMT	2.710	350.0	< 3.60 (0.00 ± 1.20)	Smith et al. 1999
		JCMT	4.760	350.0	< 4.50 (0.00 ± 1.50)	Smith et al. 1999
		JCMT	7.680	350.0	< 3.90 (0.00 ± 1.30)	Smith et al. 1999
		JCMT	Late	350.0	< 3.33 (0.49 ± 1.11)	Berger et al. 2003
		JCMT	Late	670.0	< 37.80 (−14.20 ± 12.60)	Berger et al. 2003
980326	—	JCMT	2.470	350.0	< 8.10 (0.00 ± 2.70)	Smith et al. 1999
		JCMT	Late	350.0	< 3.54 (−0.27 ± 1.18)	Tanvir et al. 2004
		JCMT	2.470	670.0	< 90.00 (0.00 ± 30.00)	Smith et al. 1999
980329	3.50	OVRO	7.800	90.0	< 2.10 (1.65 ± 0.70)	Taylor et al. 1998
		OVRO	9.800	90.0	< 2.55 (1.67 ± 0.85)	Taylor et al. 1998
		OVRO	11.800	90.0	< 2.37 (1.24 ± 0.79)	Taylor et al. 1998
		OVRO	12.800	90.0	< 2.40 (0.72 ± 0.80)	Taylor et al. 1998
		JCMT	10.000	220.0	< 3.60 (0.00 ± 1.20)	Smith et al. 1999
		JCMT	7.000	350.0	5.00 ± 1.50	Smith et al. 1999
		JCMT	8.000	350.0	4.00 ± 1.20	Smith et al. 1999
		JCMT	9.000	350.0	< 2.70 (2.10 ± 0.90)	Smith et al. 1999
		JCMT	10.000	350.0	< 3.00 (2.00 ± 1.00)	Smith et al. 1999
		JCMT	13.000	350.0	< 2.70 (0.80 ± 0.90)	Smith et al. 1999
		JCMT	Late	350.0	< 2.52 (1.83 ± 0.84)	Berger et al. 2003
		JCMT	Late	350.0	< 3.57 (−1.53 ± 1.19)	Tanvir et al. 2004
		JCMT	7.500	670.0	< 30.00 (0.00 ± 10.00)	Smith et al. 1999
		JCMT	Late	670.0	< 30.60 (8.60 ± 10.20)	Berger et al. 2003
		980519	—	JCMT	8.200	350.0
JCMT	8.200			350.0	< 240.00 (0.00 ± 80.00)	Smith et al. 1999
980613	1.10	JCMT	Late	350.0	< 2.76 (1.75 ± 0.92)	Berger et al. 2003
		JCMT	Late	670.0	< 52.80 (22.60 ± 17.60)	Berger et al. 2003

Table 1. continued.

GRB	Redshift	Observatory	$t - t_0$ (days)	Band (GHz)	Flux density (mJy)	Reference
980703	0.97	JCMT	7.320	220.0	< 7.80 (0.00 ± 2.60)	Smith et al. 1999
		JCMT	12.420	350.0	< 4.80 (0.00 ± 1.60)	Smith et al. 1999
		JCMT	Late	350.0	< 2.79 (−1.64 ± 0.93)	Berger et al. 2003
		JCMT	Late	350.0	< 3.42 (−1.36 ± 1.14)	Tanvir et al. 2004
		JCMT	12.420	670.0	< 60.00 (0.00 ± 20.00)	Smith et al. 1999
		JCMT	Late	670.0	< 32.10 (−13.90 ± 10.70)	Berger et al. 2003
981220	—	JCMT	9.330	350.0	< 4.80 (0.10 ± 1.60)	Smith et al. 1999
981226	1.11	JCMT	3.740	350.0	< 11.40 (0.60 ± 3.80)	Smith et al. 1999
		JCMT	Late	350.0	< 3.51 (−2.97 ± 1.17)	Barnard et al. 2003
990123	1.61	PDBI	1.770	86.3	< 0.87 (0.10 ± 0.29)	Galama et al. 1999
		IRAM30m	5.130	86.6	< 27.30 (−4.10 ± 9.10)	Galama et al. 1999
		IRAM30m	7.120	86.6	< 10.50 (8.50 ± 3.50)	Galama et al. 1999
		PDBI	9.060	86.3	< 0.93 (−0.50 ± 0.31)	Galama et al. 1999
		PDBI	11.650	86.3	< 1.44 (−0.03 ± 0.48)	Galama et al. 1999
		IRAM30m	5.130	142.3	< 99.00 (−37.00 ± 33.00)	Galama et al. 1999
		IRAM30m	7.120	142.3	< 87.00 (10.00 ± 29.00)	Galama et al. 1999
		JCMT	1.270	222.0	< 7.50 (−4.10 ± 2.50)	Galama et al. 1999
		PDBI	1.770	232.0	< 3.60 (−1.60 ± 1.20)	Galama et al. 1999
		JCMT	4.420	222.0	< 5.70 (0.70 ± 1.90)	Galama et al. 1999
		IRAM30m	5.130	228.9	< 57.00 (−9.00 ± 19.00)	Galama et al. 1999
		IRAM30m	7.120	228.9	< 36.00 (13.00 ± 12.00)	Galama et al. 1999
		PDBI	9.060	212.2	< 3.90 (0.40 ± 1.30)	Galama et al. 1999
		PDBI	11.650	231.5	< 12.90 (−2.70 ± 4.30)	Galama et al. 1999
		JCMT	4.480	353.0	< 3.60 (−3.30 ± 1.20)	Galama et al. 1999
		JCMT	6.470	353.0	< 4.50 (0.80 ± 1.50)	Galama et al. 1999
		JCMT	12.420	353.0	4.90 ± 1.50 <sup>a</sup>	Galama et al. 1999
		JCMT	13.440	353.0	< 3.30 (1.20 ± 1.10)	Galama et al. 1999
		JCMT	Late	350.0	< 13.65 (−4.18 ± 4.55)	Tanvir et al. 2004
		JCMT	4.470	666.0	< 51.00 (−2.00 ± 17.00)	Galama et al. 1999
JCMT	6.460	666.0	< 69.00 (−8.00 ± 23.00)	Galama et al. 1999		
JCMT	12.410	666.0	< 54.00 (15.00 ± 18.00)	Galama et al. 1999		
990308	—	JCMT	Late	350.0	< 5.25 (0.02 ± 1.75)	Tanvir et al. 2004
990506	1.31	JCMT	Late	350.0	< 4.08 (−0.25 ± 1.36)	Barnard et al. 2003
991208	0.71	OVRO	3.430	100.0	3.60 ± 0.80	Galama et al. 2000
		OVRO	5.650	100.0	3.50 ± 0.80	Galama et al. 2000
		PdBI	7.420	86.2	2.50 ± 0.50	Galama et al. 2000
		OVRO	7.530	100.0	< 2.40 (1.90 ± 0.80)	Galama et al. 2000
		OVRO	8.690	100.0	< 2.40 (1.70 ± 0.80)	Galama et al. 2000
		IRAM30m	3.570	250.0	2.60 ± 0.80	Galama et al. 2000
		IRAM30m	4.190	250.0	2.00 ± 0.50	Galama et al. 2000
		IRAM30m	6.160	250.0	< 2.10 (2.00 ± 0.70)	Galama et al. 2000
		IRAM30m	13.190	250.0	< 1.80 (0.10 ± 0.60)	Galama et al. 2000
		JCMT	7.630	350.0	< 11.10 (3.40 ± 3.70)	Smith et al. 2001
		JCMT	11.630	350.0	< 5.40 (−0.80 ± 1.80)	Smith et al. 2001
		JCMT	Late	350.0	< 3.66 (1.97 ± 1.22)	Tanvir et al. 2004
		JCMT	Late	350.0	< 3.36 (−1.04 ± 1.12)	Berger et al. 2003
		JCMT	Late	670.0	< 51.60 (26.00 ± 17.20)	Berger et al. 2003
991216	1.02	OVRO	2.630	99.0	< 2.10 (0.09 ± 0.70)	Frail et al. 2000
		JCMT	1.810	350.0	< 4.80 (0.70 ± 1.60)	Smith et al. 2001
		JCMT	2.780	350.0	< 5.10 (−2.00 ± 1.70)	Smith et al. 2001
		JCMT	Late	350.0	< 2.82 (0.47 ± 0.94)	Berger et al. 2003
		JCMT	Late	670.0	< 63.90 (−6.50 ± 21.30)	Berger et al. 2003
000210	0.85	JCMT	Late	350.0	< 4.62 (3.31 ± 1.54)	Barnard et al. 2003
		JCMT	Late	350.0	2.97 ± 0.88	Berger et al. 2003
		JCMT	Late	670.0	< 135.30 (70.10 ± 45.10)	Berger et al. 2003

Table 1. continued.

GRB	Redshift	Observatory	$t - t_0$ (days)	Band (GHz)	Flux density (mJy)	Reference
000301C	2.03	OVRO	4.160	100.0	$2.85 \pm 0.95$	Berger et al. 2000
		OVRO	5.160	100.0	$< 4.50 (0.10 \pm 1.50)$	Berger et al. 2000
		IRAM30m	2.880	250.0	$2.10 \pm 0.30$	Berger et al. 2000
		IRAM30m	4.000	250.0	$2.30 \pm 0.40$	Berger et al. 2000
		IRAM30m	4.880	250.0	$2.00 \pm 0.50$	Berger et al. 2000
		IRAM30m	7.840	250.0	$< 1.80 (0.40 \pm 0.60)$	Berger et al. 2000
		IRAM30m	22.880	250.0	$< 1.50 (-0.30 \pm 0.50)$	Berger et al. 2000
		JCMT	3.340	350.0	$< 9.30 (3.10 \pm 3.10)$	Smith et al. 2001
		JCMT	4.120	350.0	$< 3.60 (1.90 \pm 1.20)$	Smith et al. 2001
		JCMT	5.090	350.0	$< 2.70 (1.10 \pm 0.90)$	Smith et al. 2001
		JCMT	Late	350.0	$< 3.63 (-1.81 \pm 1.21)$	Tanvir et al. 2004
		JCMT	Late	350.0	$< 3.99 (-1.04 \pm 1.33)$	Berger et al. 2003
		JCMT	Late	670.0	$< 32.10 (21.40 \pm 10.70)$	Berger et al. 2003
000418	1.12	JCMT	Late	350.0	$3.15 \pm 0.90$	Berger et al. 2003
		JCMT	Late	670.0	$< 78.30 (31.90 \pm 26.10)$	Berger et al. 2003
000911	1.06	JCMT	6.230	350.0	$< 4.20 (-0.40 \pm 1.40)$	Smith et al. 2001
		JCMT	9.190	350.0	$< 3.30 (0.30 \pm 1.10)$	Smith et al. 2001
		JCMT	Late	350.0	$< 2.73 (2.31 \pm 0.91)$	Berger et al. 2003
		JCMT	Late	670.0	$< 68.10 (4.70 \pm 22.70)$	Berger et al. 2003
000926	2.07	JCMT	3.280	350.0	$< 12.60 (7.30 \pm 4.20)$	Smith et al. 2001
		JCMT	Late	350.0	$< 3.69 (1.40 \pm 1.23)$	Tanvir et al. 2004
001025A	—	JCMT	Late	350.0	$< 9.12 (-2.53 \pm 3.04)$	Tanvir et al. 2004
001109	—	IRAM30m	Late	250.0	$< 1.50 (0.00 \pm 0.50)$	Castro Cerón et al. 2004
010222	1.48	OVRO	0.400	98.5	$< 6.00 (0.30 \pm 2.00)$	Frail et al. 2002
		OVRO	1.210	98.5	$< 2.40 (-0.30 \pm 0.80)$	Frail et al. 2002
		PdBI	2.720	93.1	$< 0.96 (-0.49 \pm 0.32)$	Sagar et al. 2001
		PdBI	21.960	93.1	$< 0.69 (-0.42 \pm 0.23)$	Sagar et al. 2001
		IRAM30m	0.800	250.0	$< 1.62 (1.32 \pm 0.54)$	Frail et al. 2002
		OVRO	1.210	221.0	$< 15.00 (1.15 \pm 5.00)$	Frail et al. 2002
		PdBI	2.720	232.0	$< 4.80 (-0.09 \pm 1.60)$	Sagar et al. 2001
		IRAM30m	2.820	250.0	$1.09 \pm 0.32^b$	Frail et al. 2002
		IRAM30m	3.900	250.0	$1.00 \pm 0.33^b$	Frail et al. 2002
		IRAM30m	19.020	250.0	$< 2.82 (0.91 \pm 0.94)$	Frail et al. 2002
		IRAM30m	19.930	250.0	$< 1.83 (1.31 \pm 0.61)$	Frail et al. 2002
		PdBI	21.960	227.2	$< 4.50 (-4.57 \pm 1.50)$	Sagar et al. 2001
		IRAM30m	24.630	250.0	$< 3.30 (0.78 \pm 1.10)$	Frail et al. 2002
		IRAM30m	Late	250.0	$< 1.44 (1.13 \pm 0.48)$	Frail et al. 2002
		JCMT	0.350	350.0	$4.34 \pm 1.09^b$	Frail et al. 2002
		JCMT	1.320	350.0	$3.36 \pm 0.72^b$	Frail et al. 2002
		JCMT	2.440	350.0	$4.04 \pm 1.14^b$	Frail et al. 2002
		JCMT	7.210	350.0	$< 6.18 (1.14 \pm 2.06)$	Frail et al. 2002
JCMT	8.370	350.0	$< 2.82 (0.63 \pm 0.94)$	Frail et al. 2002		
JCMT	18.430	350.0	$3.98 \pm 1.25^b$	Frail et al. 2002		
JCMT	2.400	660.0	$< 37.80 (0.00 \pm 12.60)$	Frail et al. 2002		
010921	0.45	JCMT	Late	350.0	$< 3.42 (0.46 \pm 1.14)$	Tanvir et al. 2004
011211	2.14	JCMT	Late	350.0	$< 3.03 (1.39 \pm 1.01)$	Berger et al. 2003
		JCMT	Late	350.0	$< 5.61 (3.81 \pm 1.87)$	Tanvir et al. 2004
		JCMT	Late	670.0	$< 45.60 (8.10 \pm 15.20)$	Berger et al. 2003
020124	3.20	IRAM30m	Late	250.0	$< 1.80 (0.28 \pm 0.60)$	Priddey et al. 2006
		JCMT	Late	350.0	$< 6.90 (1.20 \pm 2.30)$	Tanvir et al. 2004
020531	—	PdBI	20.833	86.2	$< 3.15 (-0.38 \pm 1.05)$	Castro-Tirado et al. (in prep.)
020813	—	PdBI	0.850	89.2	$< 1.11 (-0.13 \pm 0.37)$	Bremer & Castro-Tirado 2002
		IRAM30m	0.730	250.0	$< 3.45 (1.45 \pm 1.15)$	Bertoldi et al. 2002
		PdBI	0.850	232.0	$< 6.18 (-0.63 \pm 2.06)$	Bremer & Castro-Tirado 2002
		IRAM30m	1.870	250.0	$< 4.17 (1.08 \pm 1.39)$	Bertoldi et al. 2002
		JCMT	Late	350.0	$< 10.50 (-1.40 \pm 3.50)$	Tanvir et al. 2004

Table 1. continued.

GRB	Redshift	Observatory	$t - t_0$ (days)	Band (GHz)	Flux density (mJy)	Reference
021004	2.32	PdBI	1.480	86.3	$2.47 \pm 0.29$	de Ugarte Postigo et al. 2005
		PdBI	1.641	115.3	$< 4.32 (1.62 \pm 1.44)$	de Ugarte Postigo et al. 2005
		PdBI	2.639	87.7	$2.57 \pm 0.56$	de Ugarte Postigo et al. 2005
		PdBI	6.477	86.2	$1.67 \pm 0.34$	de Ugarte Postigo et al. 2005
		PdBI	15.414	92.0	$0.97 \pm 0.25$	de Ugarte Postigo et al. 2005
		PdBI	32.477	98.0	$< 0.81 (0.15 \pm 0.27)$	de Ugarte Postigo et al. 2005
		PdBI	1.480	231.7	$< 3.66 (1.22 \pm 1.22)$	de Ugarte Postigo et al. 2005
		PdBI	1.641	231.7	$< 10.95 (0.22 \pm 3.65)$	de Ugarte Postigo et al. 2005
		PdBI	2.639	232.0	$< 4.62 (3.26 \pm 1.54)$	de Ugarte Postigo et al. 2005
		PdBI	6.477	208.5	$< 5.88 (4.71 \pm 1.96)$	de Ugarte Postigo et al. 2005
		PdBI	15.414	232.0	$< 3.00 (1.60 \pm 1.00)$	de Ugarte Postigo et al. 2005
		PdBI	32.477	239.6	$< 2.13 (-0.33 \pm 0.71)$	de Ugarte Postigo et al. 2005
		JCMT	0.140	350.0	$< 78.00 (5.00 \pm 26.00)$	Smith et al. 2005a
		JCMT	0.853	350.0	$< 15.00 (-4.00 \pm 5.00)$	Smith et al. 2005a
		JCMT	1.913	350.0	$< 4.50 (0.90 \pm 1.50)$	Smith et al. 2005a
		JCMT	6.984	350.0	$< 4.50 (-3.70 \pm 1.50)$	Smith et al. 2005a
JCMT	Late	350.0	$< 3.75 (0.77 \pm 1.25)$	Tanvir et al. 2004		
021211	1.01	IRAM30m	Late	250.0	$< 1.59 (0.07 \pm 0.53)$	Priddey et al. 2006
		JCMT	1.033	350.0	$< 7.50 (2.10 \pm 2.50)$	Smith et al. 2005a
		JCMT	9.973	350.0	$< 9.00 (-2.40 \pm 3.00)$	Smith et al. 2005a
030115	—	IRAM30m	0.940	250.0	$< 2.70 (0.40 \pm 0.90)$	Bertoldi et al. 2003b
		IRAM30m	3.170	250.0	$< 4.80 (2.90 \pm 1.60)$	Bertoldi et al. 2003b
		IRAM30m	Late	250.0	$< 2.28 (0.01 \pm 0.76)$	Priddey et al. 2006
		JCMT	Late	250.0	$< 3.30 (-1.00 \pm 1.10)$	Priddey et al. 2006
		JCMT	3.314	350.0	$< 5.40 (0.20 \pm 1.80)$	Smith et al. 2005a
		JCMT	Late	670.0	$< 36.00 (-1.00 \pm 12.00)$	Priddey et al. 2006
030226	1.99	PdBI	1.799	85.3	$< 0.93 (0.54 \pm 0.31)$	Pandey et al. 2004
		PdBI	4.042	89.2	$< 2.28 (-0.50 \pm 0.76)$	Pandey et al. 2004
		PdBI	10.049	92.0	$< 2.10 (-1.01 \pm 0.70)$	Pandey et al. 2004
		PdBI	12.009	90.8	$< 2.52 (-0.43 \pm 0.84)$	Pandey et al. 2004
		PdBI	13.751	114.7	$< 2.04 (0.73 \pm 0.68)$	Pandey et al. 2004
		PdBI	16.785	92.1	$< 1.02 (0.23 \pm 0.34)$	Pandey et al. 2004
		PdBI	1.799	220.3	$< 5.88 (-0.90 \pm 1.96)$	Pandey et al. 2004
		PdBI	10.049	232.0	$< 10.35 (-0.83 \pm 3.45)$	Pandey et al. 2004
		PdBI	12.009	221.9	$< 11.58 (-4.00 \pm 3.86)$	Pandey et al. 2004
		PdBI	13.751	231.0	$< 4.53 (-2.13 \pm 1.51)$	Pandey et al. 2004
		PdBI	16.785	219.0	$< 3.36 (-0.25 \pm 1.12)$	Pandey et al. 2004
		IRAM30m	Late	250.0	$< 1.98 (-0.29 \pm 0.66)$	Priddey et al. 2006
		JCMT	0.245	350.0	$< 7.80 (5.10 \pm 2.60)$	Smith et al. 2005a
		JCMT	0.301	350.0	$< 3.90 (1.20 \pm 1.30)$	Smith et al. 2005a
JCMT	1.288	350.0	$< 5.40 (-1.90 \pm 1.80)$	Smith et al. 2005a		
JCMT	2.369	350.0	$< 4.50 (0.00 \pm 1.50)$	Smith et al. 2005a		
JCMT	24.401	350.0	$< 11.40 (-4.30 \pm 3.80)$	Smith et al. 2005a		
030227	—	IRAM30m	Late	250.0	$< 1.59 (-0.57 \pm 0.53)$	Priddey et al. 2006
030329	0.17	SEST	0.500	86.0	$< 156.00 (82.00 \pm 52.00)$	Resmi et al. 2005
		OVRO	0.663	98.0	$50.90 \pm 1.60$	Sheth et al. 2003
		OVRO	0.746	98.0	$60.00 \pm 1.40$	Sheth et al. 2003
		OVRO	0.830	98.0	$61.70 \pm 1.90$	Sheth et al. 2003
		OVRO	0.926	98.0	$57.60 \pm 1.60$	Sheth et al. 2003
		SEST	1.500	86.0	$< 234.00 (-2.00 \pm 78.00)$	Resmi et al. 2005
		PdBI	1.582	86.2	$58.60 \pm 0.50$	Resmi et al. 2005
		OVRO	1.716	98.0	$59.60 \pm 1.60$	Sheth et al. 2003
		OVRO	1.799	98.0	$62.30 \pm 1.70$	Sheth et al. 2003
		OVRO	1.871	98.0	$59.30 \pm 2.00$	Sheth et al. 2003
		PdBI	2.401	98.5	$58.20 \pm 0.60$	Resmi et al. 2005
		SEST	2.500	86.0	$< 195.00 (38.00 \pm 65.00)$	Resmi et al. 2005
		OVRO	2.862	98.0	$70.00 \pm 6.00$	Sheth et al. 2003
		PdBI	3.396	86.7	$51.70 \pm 0.90$	Resmi et al. 2005
		OVRO	3.635	98.0	$55.40 \pm 1.80$	Sheth et al. 2003
		OVRO	3.760	98.0	$66.50 \pm 2.10$	Sheth et al. 2003
OVRO	3.891	98.0	$54.60 \pm 2.40$	Sheth et al. 2003		

Table 1. continued.

GRB	Redshift	Observatory	$t - t_0$ (days)	Band (GHz)	Flux density (mJy)	Reference
		OVRO	4.779	98.0	$48.40 \pm 1.30$	Sheth et al. 2003
		NRO45m	5.090	90.0	$65.00 \pm 9.00$	Kuno et al. 2004
		NRO45m	5.140	90.0	$67.00 \pm 9.00$	Kuno et al. 2004
		OVRO	5.800	98.0	$53.90 \pm 0.90$	Sheth et al. 2003
		BIMA	6.833	98.0	$59.00 \pm 2.00$	Sheth et al. 2003
		PdBI	7.244	115.0	$40.40 \pm 3.70$	Resmi et al. 2005
		BIMA	7.857	98.0	$47.00 \pm 2.00$	Sheth et al. 2003
		NRO45m	8.030	90.0	$36.00 \pm 10.00$	Kuno et al. 2004
		BIMA	9.645	98.0	$41.00 \pm 5.00$	Sheth et al. 2003
		BIMA	10.709	98.0	$33.00 \pm 3.00$	Sheth et al. 2003
		BIMA	11.652	98.0	$21.00 \pm 4.00$	Sheth et al. 2003
		OVRO	11.747	98.0	$25.80 \pm 3.10$	Sheth et al. 2003
		NRO45m	12.070	90.0	$< 20.10 (0.00 \pm 6.70)$	Kuno et al. 2004
		NMA	12.150	93.0	$18.70 \pm 2.10$	Kohno et al. 2005
		PdBI	12.285	86.2	$23.50 \pm 0.40$	Resmi et al. 2005
		BIMA	12.680	98.0	$22.00 \pm 4.00$	Sheth et al. 2003
		OVRO	12.752	98.0	$19.70 \pm 4.00$	Sheth et al. 2003
		BIMA	13.606	98.0	$25.00 \pm 4.00$	Sheth et al. 2003
		NMA	15.050	93.0	$17.80 \pm 1.90$	Kohno et al. 2005
		BIMA	15.695	98.0	$14.00 \pm 4.00$	Sheth et al. 2003
		PdBI	16.400	91.3	$14.90 \pm 0.40$	Resmi et al. 2005
		BIMA	16.887	98.0	$15.00 \pm 4.00$	Sheth et al. 2003
		NMA	17.110	93.0	$16.10 \pm 3.10$	Kohno et al. 2005
		BIMA	17.727	98.0	$11.00 \pm 3.00$	Sheth et al. 2003
		NMA	18.070	93.0	$9.10 \pm 1.90$	Kohno et al. 2005
		NRO45m	19.040	90.0	$< 27.90 (0.00 \pm 9.30)$	Kuno et al. 2004
		PdBI	20.366	115.0	$7.70 \pm 1.00$	Resmi et al. 2005
		NMA	21.100	93.0	$< 12.60 (8.80 \pm 4.20)$	Kohno et al. 2005
		NMA	23.060	93.0	$8.90 \pm 1.30$	Kohno et al. 2005
		PdBI	26.289	96.2	$4.70 \pm 0.70$	Resmi et al. 2005
		BIMA	31.773	98.0	$< 3.00 (0.00 \pm 1.00)$	Sheth et al. 2003
		NMA	32.020	93.0	$< 8.40 (0.00 \pm 2.80)$	Kohno et al. 2005
		PdBI	35.262	86.2	$2.90 \pm 0.30$	Resmi et al. 2005
		PdBI	48.126	86.2	$< 2.40 (1.10 \pm 0.80)$	Resmi et al. 2005
		NMA	52.990	93.0	$< 3.90 (0.00 \pm 1.30)$	Kohno et al. 2005
		PdBI	60.450	84.4	$< 2.10 (0.40 \pm 0.70)$	Resmi et al. 2005
		NMA	60.980	93.0	$< 6.00 (0.00 \pm 2.00)$	Kohno et al. 2005
		NMA	61.970	93.0	$< 5.10 (0.00 \pm 1.70)$	Kohno et al. 2005
		PdBI	83.151	95.4	$< 3.90 (0.60 \pm 1.30)$	Resmi et al. 2005
		NMA	8.230	141.0	$41.00 \pm 3.20$	Kohno et al. 2005
		NMA	9.070	141.0	$42.50 \pm 2.40$	Kohno et al. 2005
		SEST	0.500	215.0	$< 924.00 (201.00 \pm 308.00)$	Resmi et al. 2005
		IRAM30m	1.447	250.0	$49.20 \pm 1.10$	Sheth et al. 2003
		SEST	1.500	215.0	$< 786.00 (-49.00 \pm 262.00)$	Resmi et al. 2005
		PdBI	1.582	232.0	$46.80 \pm 3.10$	Resmi et al. 2005
		PdBI	2.401	238.0	$40.60 \pm 2.10$	Resmi et al. 2005
		SEST	2.500	215.0	$< 750.00 (-144.00 \pm 250.00)$	Resmi et al. 2005
		PdBI	3.396	241.0	$23.80 \pm 3.20$	Resmi et al. 2005
		IRAM30m	3.804	250.0	$45.70 \pm 3.20$	Sheth et al. 2003
		IRAM30m	4.479	250.0	$36.20 \pm 2.30$	Sheth et al. 2003
		IRAM30m	5.536	250.0	$41.60 \pm 1.60$	Sheth et al. 2003
		IRAM30m	6.376	250.0	$46.40 \pm 1.60$	Sheth et al. 2003
		IRAM30m	7.428	250.0	$32.00 \pm 1.80$	Sheth et al. 2003
		IRAM30m	8.486	250.0	$25.50 \pm 1.80$	Sheth et al. 2003
		PdBI	12.285	232.0	$12.80 \pm 1.30$	Resmi et al. 2005
		IRAM30m	16.328	250.0	$9.30 \pm 2.30$	Sheth et al. 2003
		PdBI	16.400	217.0	$9.20 \pm 2.20$	Resmi et al. 2005
		PdBI	20.366	232.0	$6.50 \pm 1.80$	Resmi et al. 2005
		IRAM30m	22.318	250.0	$5.20 \pm 1.10$	Sheth et al. 2003
		PdBI	26.289	241.0	$< 11.40 (0.00 \pm 3.80)$	Resmi et al. 2005
		PdBI	35.262	233.0	$< 3.90 (1.40 \pm 1.30)$	Resmi et al. 2005
		PdBI	48.126	231.0	$< 30.30 (0.00 \pm 10.10)$	Resmi et al. 2005
		PdBI	60.450	238.0	$< 24.00 (0.00 \pm 8.00)$	Resmi et al. 2005
		JCMT	4.914	350.0	$37.80 \pm 4.50$	Smith et al. 2005b
		JCMT	5.901	350.0	$27.60 \pm 2.90$	Smith et al. 2005b
		JCMT	6.801	350.0	$33.90 \pm 2.80$	Smith et al. 2005b

Table 1. continued.

GRB	Redshift	Observatory	$t - t_0$ (days)	Band (GHz)	Flux density (mJy)	Reference
		JCMT	10.760	350.0	< 15.30 (10.90 ± 5.10)	Smith et al. 2005b
		JCMT	16.754	350.0	< 5.70 (-0.20 ± 1.90)	Smith et al. 2005b
		JCMT	17.870	350.0	< 8.10 (-1.90 ± 2.70)	Smith et al. 2005b
031026	—	IRAM30m	7.000	250.0	< 12.00 (0.00 ± 4.00)	Bertoldi et al. 2003a
031203	0.10	APEX	Late	345.0	< 6.60 (4.00 ± 2.20)	Watson et al. 2011
041006	0.72	JCMT	0.098	350.0	< 15.00 (2.00 ± 5.00)	Smith et al. 2005a
		JCMT	0.969	350.0	< 3.90 (0.90 ± 1.30)	Smith et al. 2005a
041219A	0.31	PdBI	2.551	86.2	< 0.81 (0.77 ± 0.27)	Castro-Tirado et al. (in prep.)
		PdBI	4.320	99.2	1.18 ± 0.38	Castro-Tirado et al. (in prep.)
		PdBI	10.492	86.3	< 1.41 (0.59 ± 0.47)	Castro-Tirado et al. (in prep.)
		PdBI	11.755	86.3	< 0.90 (0.02 ± 0.30)	Castro-Tirado et al. (in prep.)
		PdBI	2.551	232.0	< 2.64 (0.93 ± 0.88)	Castro-Tirado et al. (in prep.)
		PdBI	4.320	240.0	< 3.15 (0.03 ± 1.05)	Castro-Tirado et al. (in prep.)
050306	—	IRAM30m	2.206	250.0	< 1.65 (0.26 ± 0.55)	Bertoldi et al. 2005
050408	1.24	PdBI	3.230	86.8	< 0.90 (0.00 ± 0.30)	de Ugarte Postigo et al. 2007
		PdBI	5.190	115.0	< 2.40 (0.50 ± 0.80)	de Ugarte Postigo et al. 2007
		PdBI	10.340	86.3	< 0.90 (0.90 ± 0.30)	de Ugarte Postigo et al. 2007
		PdBI	11.190	109.0	< 5.10 (-1.70 ± 1.70)	de Ugarte Postigo et al. 2007
		PdBI	12.400	109.0	< 2.10 (-0.90 ± 0.70)	de Ugarte Postigo et al. 2007
		PdBI	14.290	112.0	< 1.20 (-0.80 ± 0.40)	de Ugarte Postigo et al. 2007
		PdBI	3.230	229.0	< 4.80 (1.00 ± 1.60)	de Ugarte Postigo et al. 2007
		PdBI	5.190	232.0	< 5.40 (3.30 ± 1.80)	de Ugarte Postigo et al. 2007
		PdBI	10.340	232.0	8.40 ± 2.30 <sup>c</sup>	de Ugarte Postigo et al. 2007
		PdBI	11.190	229.0	< 19.50 (-9.90 ± 6.50)	de Ugarte Postigo et al. 2007
		PdBI	12.400	229.0	< 8.10 (3.60 ± 2.70)	de Ugarte Postigo et al. 2007
		PdBI	14.290	225.0	< 6.30 (1.40 ± 2.10)	de Ugarte Postigo et al. 2007
050416A	0.65	PdBI	13.208	86.2	< 0.66 (0.20 ± 0.22)	Castro-Tirado et al. (in prep.)
050509B	0.22	PdBI	1.970	80.3	< 5.70 (0.00 ± 1.90)	Castro-Tirado et al. 2005
		PdBI	2.780	80.5	< 2.40 (0.00 ± 0.80)	Castro-Tirado et al. 2005
		PdBI	3.899	80.5	< 3.00 (0.00 ± 1.00)	Castro-Tirado et al. 2005
		PdBI	7.667	92.7	< 0.90 (0.00 ± 0.30)	Castro-Tirado et al. 2005
		PdBI	1.970	243.0	< 36.00 (0.00 ± 12.00)	Castro-Tirado et al. 2005
		PdBI	2.780	243.0	< 17.70 (0.00 ± 5.90)	Castro-Tirado et al. 2005
		PdBI	3.899	222.0	< 13.20 (0.00 ± 4.40)	Castro-Tirado et al. 2005
050525	—	PdBI	1.131	92.7	< 1.02 (0.54 ± 0.34)	Castro-Tirado et al. (in prep.)
		PdBI	1.131	214.0	< 3.66 (1.29 ± 1.22)	Castro-Tirado et al. (in prep.)
050603	2.82	JCMT	0.510	350.0	< 6.00 (2.40 ± 2.00)	Barnard et al. 2005
		JCMT	0.510	670.0	< 285.00 (-42.00 ± 95.00)	Barnard et al. 2005
050730	3.97	PdBI	2.905	103.0	< 2.82 (2.74 ± 0.94)	Pandey et al. 2006
		PdBI	5.875	105.0	< 1.53 (1.34 ± 0.51)	Pandey et al. 2006
		PdBI	Late	86.8	< 0.81 (-0.24 ± 0.27)	Pandey et al. 2006
		PdBI	2.905	213.0	< 12.63 (4.39 ± 4.21)	Pandey et al. 2006
		PdBI	5.875	215.0	< 11.43 (-5.13 ± 3.81)	Pandey et al. 2006
		PdBI	Late	231.0	< 5.79 (-4.21 ± 1.93)	Pandey et al. 2006
050904	6.29	PdBI	5.896	89.3	1.45 ± 0.47	Castro-Tirado et al. (in prep.)
		PdBI	5.896	238.0	< 13.11 (3.90 ± 4.37)	Castro-Tirado et al. (in prep.)
		IRAM30m	Late	250.0	< 1.35 (-0.76 ± 0.45)	Walter et al. 2006
051022	0.81	PdBI	1.373	90.8	1.14 ± 0.28	Castro-Tirado et al. 2007
		PdBI	2.391	86.2	< 0.51 (0.08 ± 0.17)	Castro-Tirado et al. 2007
		PdBI	6.415	86.2	< 1.32 (-0.33 ± 0.44)	Castro-Tirado et al. 2007
		PdBI	8.157	90.2	3.48 ± 1.05	Castro-Tirado et al. 2007
		PdBI	10.235	86.2	< 0.78 (-0.50 ± 0.26)	Castro-Tirado et al. 2007
		PdBI	1.373	218.0	< 5.04 (0.02 ± 1.68)	Castro-Tirado et al. 2007
		PdBI	2.391	232.0	< 2.55 (-2.42 ± 0.85)	Castro-Tirado et al. 2007
		PdBI	6.415	232.0	< 10.20 (1.81 ± 3.40)	Castro-Tirado et al. 2007
		PdBI	10.235	222.0	< 4.05 (0.55 ± 1.35)	Castro-Tirado et al. 2007

Table 1. continued.

GRB	Redshift	Observatory	$t - t_0$ (days)	Band (GHz)	Flux density (mJy)	Reference
051105A	—	PdBI	0.546	114.7	$< 6.90 (0.00 \pm 2.30)$	Castro-Tirado et al. (in prep.)
		PdBI	1.129	114.7	$< 9.00 (0.00 \pm 3.00)$	Castro-Tirado et al. (in prep.)
		PdBI	0.546	230.5	$< 1.89 (0.00 \pm 0.63)$	Castro-Tirado et al. (in prep.)
		PdBI	0.546	230.5	$< 3.30 (0.00 \pm 1.10)$	Castro-Tirado et al. (in prep.)
060116	—	PdBI	3.502	99.2	$< 0.93 (-0.11 \pm 0.31)$	Castro-Tirado et al. (in prep.)
		PdBI	6.569	94.7	$< 0.78 (-0.14 \pm 0.26)$	Castro-Tirado et al. (in prep.)
		PdBI	3.502	231.0	$< 3.90 (0.48 \pm 1.30)$	Castro-Tirado et al. (in prep.)
		PdBI	6.569	227.0	$< 2.52 (-0.28 \pm 0.84)$	Castro-Tirado et al. (in prep.)
060218	0.03	PdBI	2.668	115.2	$< 2.01 (0.15 \pm 0.67)$	Castro-Tirado et al. (in prep.)
		PdBI	4.671	110.5	$< 2.25 (-0.64 \pm 0.75)$	Castro-Tirado et al. (in prep.)
		PdBI	6.633	94.2	$< 2.94 (0.76 \pm 0.98)$	Castro-Tirado et al. (in prep.)
		PdBI	2.668	230.0	$< 2.28 (0.46 \pm 0.76)$	Castro-Tirado et al. (in prep.)
		PdBI	4.671	220.0	$< 6.00 (-1.90 \pm 2.00)$	Castro-Tirado et al. (in prep.)
060515	—	PdBI	4.407	86.0	$< 0.72 (0.35 \pm 0.24)$	Castro-Tirado et al. (in prep.)
		PdBI	4.407	226.0	$< 3.87 (1.21 \pm 1.29)$	Castro-Tirado et al. (in prep.)
060801	1.13	PdBI	0.243	93.2	$< 1.29 (-0.16 \pm 0.43)$	Castro-Tirado et al. (in prep.)
060805B	—	PdBI	5.314	100.2	$< 1.17 (0.89 \pm 0.39)$	Castro-Tirado et al. (in prep.)
		PdBI	5.314	211.4	$< 4.80 (-1.15 \pm 1.60)$	Castro-Tirado et al. (in prep.)
060904B	0.70	PdBI	3.438	92.3	$1.08 \pm 0.27$	Castro-Tirado et al. (in prep.)
		PdBI	6.034	90.0	$< 1.59 (0.14 \pm 0.53)$	Castro-Tirado et al. (in prep.)
		PdBI	8.021	90.0	$< 1.89 (0.67 \pm 0.63)$	Castro-Tirado et al. (in prep.)
		PdBI	3.438	211.1	$< 8.16 (0.60 \pm 2.72)$	Castro-Tirado et al. (in prep.)
		PdBI	6.034	211.1	$< 14.10 (4.39 \pm 4.70)$	Castro-Tirado et al. (in prep.)
		PdBI	8.021	211.1	$< 19.02 (8.09 \pm 6.34)$	Castro-Tirado et al. (in prep.)
060908	1.88	PdBI	0.708	92.0	$< 0.90 (0.00 \pm 0.30)$	<a href="#">Covino et al. 2010</a>
		PdBI	0.708	236.0	$< 9.90 (0.00 \pm 3.30)$	<a href="#">Covino et al. 2010</a>
070125	1.55	PdBI	2.590	100.0	$2.21 \pm 0.13$	Castro-Tirado et al. (in prep.)
		PdBI	5.740	100.0	$1.95 \pm 0.16$	Castro-Tirado et al. (in prep.)
		PdBI	6.650	100.0	$1.80 \pm 0.20$	Castro-Tirado et al. (in prep.)
		PdBI	8.670	100.0	$1.66 \pm 0.19$	Castro-Tirado et al. (in prep.)
		CARMA	10.980	95.0	$2.30 \pm 0.70$	<a href="#">Chandra et al. 2008</a>
		PdBI	14.790	100.0	$1.23 \pm 0.20$	Castro-Tirado et al. (in prep.)
		CARMA	14.960	95.0	$1.34 \pm 0.16$	<a href="#">Chandra et al. 2008</a>
		PdBI	16.790	100.0	$1.15 \pm 0.20$	Castro-Tirado et al. (in prep.)
		CARMA	17.900	95.0	$2.10 \pm 0.70$	<a href="#">Chandra et al. 2008</a>
		PdBI	21.790	100.0	$1.05 \pm 0.20$	Castro-Tirado et al. (in prep.)
		CARMA	23.960	95.0	$2.40 \pm 0.70$	<a href="#">Chandra et al. 2008</a>
		PdBI	37.730	100.0	$< 0.63 (0.41 \pm 0.21)$	Castro-Tirado et al. (in prep.)
		IRAM30m	6.520	250.0	$3.14 \pm 0.59$	<a href="#">Chandra et al. 2008</a>
		IRAM30m	7.610	250.0	$< 2.16 (1.91 \pm 0.72)$	<a href="#">Chandra et al. 2008</a>
IRAM30m	10.610	250.0	$< 2.13 (1.47 \pm 0.71)$	<a href="#">Chandra et al. 2008</a>		
IRAM30m	16.480	250.0	$< 2.79 (2.67 \pm 0.93)$	<a href="#">Chandra et al. 2008</a>		
IRAM30m	18.480	250.0	$< 2.79 (1.27 \pm 0.93)$	<a href="#">Chandra et al. 2008</a>		
070219	—	PdBI	3.770	80.7	$< 0.54 (0.16 \pm 0.18)$	Castro-Tirado et al. (in prep.)
070223	—	PdBI	12.000	90.0	$< 0.54 (0.00 \pm 0.18)$	Castro-Tirado et al. (in prep.)
070306	1.50	PdBI	2.177	86.1	$1.35 \pm 0.31$	Castro-Tirado et al. (in prep.)
070531	—	PdBI	6.350	92.2	$< 1.44 (0.91 \pm 0.48)$	Castro-Tirado et al. (in prep.)
071003	1.60	PdBI	1.451	86.2	$1.30 \pm 0.20$	Castro-Tirado et al. (in prep.)
		PdBI	3.617	86.2	$< 0.39 (0.27 \pm 0.13)$	Castro-Tirado et al. (in prep.)
071010B	0.95	PdBI	10.178	100.8	$< 0.54 (0.17 \pm 0.18)$	Castro-Tirado et al. (in prep.)
071021	—	PdBI	2.375	86.0	$< 0.45 (0.00 \pm 0.15)$	Castro-Tirado et al. (in prep.)
		PdBI	4.375	86.0	$< 0.45 (0.00 \pm 0.15)$	Castro-Tirado et al. (in prep.)
		PdBI	11.375	104.8	$< 0.51 (0.00 \pm 0.17)$	Castro-Tirado et al. (in prep.)

Table 1. continued.

GRB	Redshift	Observatory	$t - t_0$ (days)	Band (GHz)	Flux density (mJy)	Reference
080109	0.0065	PdBI	14.290	90.9	$0.65 \pm 0.15$	Gorosabel et al. 2010
		PdBI	Late	103.0	$< 0.30 (0.03 \pm 0.10)$	Gorosabel et al. 2010
		IRAM30m	16.367	250.0	$2.46 \pm 0.54$	Gorosabel et al. 2010
		IRAM30m	18.636	250.0	$< 3.60 (2.29 \pm 1.20)$	Gorosabel et al. 2010
		IRAM30m	20.607	250.0	$< 1.80 (1.44 \pm 0.60)$	Gorosabel et al. 2010
080129	4.35	IRAM30m	1.645	250.0	$2.98 \pm 0.63$	Greiner et al. 2009
		IRAM30m	2.725	250.0	$< 1.41 (1.27 \pm 0.47)$	Greiner et al. 2009
		IRAM30m	4.765	250.0	$< 1.50 (1.16 \pm 0.50)$	Greiner et al. 2009
		IRAM30m	8.735	250.0	$< 1.65 (-0.40 \pm 0.55)$	Greiner et al. 2009
		IRAM30m	11.800	250.0	$< 3.42 (0.55 \pm 1.14)$	Greiner et al. 2009
080205	—	PdBI	2.010	91.7	$< 0.57 (0.00 \pm 0.19)$	Castro-Tirado et al. (in prep.)
080207	~1.74	JCMT	Late	353.0	$< 13.12 (2.53 \pm 4.37)$	Svensson et al. 2011
		JCMT	Late	667.0	$< 53.22 (23.04 \pm 17.74)$	Svensson et al. 2011
080319B	0.94	PdBI	0.991	97.0	$0.41 \pm 0.12$	Racusin et al. 2008
		CARMA	1.110	95.0	$< 0.75 (0.12 \pm 0.25)$	Benko et al. 2010
		PdBI	3.991	97.0	$< 0.57 (0.35 \pm 0.19)$	Pandey et al. 2009
		PdBI	7.991	97.0	$< 0.27 (0.20 \pm 0.09)$	Pandey et al. 2009
080426	—	PdBI	3.561	86.2	$< 0.78 (-0.20 \pm 0.26)$	Castro-Tirado et al. (in prep.)
080430	0.77	PdBI	0.739	89.9	$< 0.54 (0.00 \pm 0.18)$	de Ugarte Postigo et al. 2011f
		PdBI	2.248	96.6	$< 0.27 (0.00 \pm 0.09)$	Castro-Tirado et al. (in prep.)
		PdBI	8.816	85.4	$< 0.24 (0.00 \pm 0.08)$	Castro-Tirado et al. (in prep.)
080514B	—	PdBI	3.920	86.0	$< 0.57 (0.00 \pm 0.19)$	Rossi et al. 2008
080603B	2.69	PdBI	2.347	100.8	$< 0.48 (0.00 \pm 0.16)$	Castro-Tirado et al. (in prep.)
080721	2.60	PdBI	3.315	86.2	$< 0.60 (0.00 \pm 0.20)$	Castro-Tirado et al. (in prep.)
080913	6.70	PdBI	2.817	99.0	$< 0.72 (0.00 \pm 0.24)$	Pérez-Ramírez et al. 2010
		PdBI	7.917	84.0	$< 1.44 (0.00 \pm 0.48)$	Pérez-Ramírez et al. 2010
		PdBI	16.817	106.0	$< 0.90 (0.00 \pm 0.30)$	Pérez-Ramírez et al. 2010
		IRAM30m	30.000	250.0	$< 1.35 (0.34 \pm 0.45)$	Riechers et al. 2009a
081024	—	PdBI	0.387	86.2	$< 0.57 (0.04 \pm 0.19)$	Castro-Tirado et al. (in prep.)
090313	3.38	CARMA	1.010	92.0	$4.00 \pm 0.60$	Bock et al. 2009a
		PdBI	4.570	105.0	$1.68 \pm 0.15$	Melandri et al. 2010
		PdBI	13.590	87.0	$0.67 \pm 0.13$	Melandri et al. 2010
		PdBI	19.540	110.0	$< 0.90 (-0.21 \pm 0.30)$	Melandri et al. 2010
		PdBI	5.630	228.0	$< 1.53 (0.60 \pm 0.51)$	Melandri et al. 2010
		APEX	4.120	345.0	$< 14.10 (0.00 \pm 4.70)$	Melandri et al. 2010
APEX	11.120	345.0	$< 14.10 (0.00 \pm 4.70)$	Melandri et al. 2010		
090323	3.57	PdBI	3.831	87.2	$< 0.48 (0.00 \pm 0.16)$	Castro-Tirado et al. (in prep.)
090404	—	PdBI	1.236	108.0	$1.10 \pm 0.35$	Castro-Tirado et al. 2009a
		PdBI	3.408	87.0	$0.62 \pm 0.11$	Castro-Tirado et al. (in prep.)
090407	—	PdBI	2.042	86.2	$< 0.60 (0.00 \pm 0.20)$	Castro-Tirado et al. (in prep.)
090417B	0.34	PdBI	Late	86.2	$< 0.51 (-0.03 \pm 0.17)$	Castro-Tirado et al. (in prep.)
090423	8.20	PdBI	0.384	97.2	$0.24 \pm 0.08$	Castro-Tirado et al. 2009b
		PdBI	1.291	97.1	$0.24 \pm 0.07$	Castro-Tirado et al. 2009b
		PdBI	8.291	97.0	$< 0.24 (0.00 \pm 0.08)$	Castro-Tirado et al. 2009b
		CARMA	1.870	92.5	$< 0.54 (0.45 \pm 0.18)$	Chandra et al. 2010
		CARMA	8.291	97.0	$< 0.70 (0.00 \pm 0.23)$	Bock et al. 2009b
		IRAM30m	2.441	250.0	$< 0.96 (0.23 \pm 0.32)$	Riechers et al. 2009b
090709A	—	CARMA	5.980	88.5	$< 1.08 (0.00 \pm 0.36)$	Morgan & Bower 2009
		PdBI	6.781	86.2	$< 0.39 (0.00 \pm 0.13)$	Castro-Tirado et al. (in prep.)
090726	2.71	PdBI	1.125	91.4	$< 0.45 (0.00 \pm 0.15)$	Castro-Tirado et al. (in prep.)
091010	—	PdBI	5.708	91.0	$< 0.69 (0.00 \pm 0.23)$	Castro-Tirado et al. (in prep.)

Table 1. continued.

GRB	Redshift	Observatory	$t - t_0$ (days)	Band (GHz)	Flux density (mJy)	Reference
091102	—	APEX	0.583	345.0	$< 18.90 (0.00 \pm 6.30)$	<a href="#">de Ugarte Postigo et al. 2009a</a>
091127	0.49	APEX	0.207	345.0	$< 14.90 (0.00 \pm 4.97)$	<a href="#">de Ugarte Postigo et al. 2009b</a>
		APEX	1.150	345.0	$< 13.20 (0.00 \pm 4.40)$	<a href="#">de Ugarte Postigo et al. 2009b</a>
091208B	1.06	IRAM30m	1.666	250.0	$< 9.00 (0.00 \pm 3.00)$	Castro-Tirado et al. (in prep.)
100205A	—	PdBI	3.750	82.9	$< 0.75 (0.06 \pm 0.25)$	Castro-Tirado et al. (in prep.)
100316A	—	PdBI	0.791	86.2	$< 0.21 (0.19 \pm 0.07)$	Castro-Tirado et al. (in prep.)
100418A	0.62	PdBI	1.260	103.0	$6.57 \pm 0.07$	de Ugarte Postigo et al. (in prep.)
		PdBI	5.211	86.7	$3.70 \pm 0.07$	de Ugarte Postigo et al. (in prep.)
		PdBI	7.393	86.7	$2.26 \pm 0.13$	de Ugarte Postigo et al. (in prep.)
		PdBI	12.328	106.0	$1.13 \pm 0.12$	de Ugarte Postigo et al. (in prep.)
		PdBI	16.108	86.7	$1.14 \pm 0.05$	de Ugarte Postigo et al. (in prep.)
		PdBI	23.177	86.7	$1.18 \pm 0.09$	de Ugarte Postigo et al. (in prep.)
		PdBI	39.144	103.0	$0.61 \pm 0.13$	de Ugarte Postigo et al. (in prep.)
		PdBI	59.958	86.7	$0.58 \pm 0.18$	de Ugarte Postigo et al. (in prep.)
		PdBI	69.237	99.5	$< 0.57 (0.36 \pm 0.19)$	de Ugarte Postigo et al. (in prep.)
		SMA	0.811	345.0	$13.40 \pm 1.60$	<a href="#">Martin et al. 2010</a>
		SMA	1.745	345.0	$5.10 \pm 0.90$	de Ugarte Postigo et al. (in prep.)
		SMA	2.789	345.0	$5.40 \pm 1.10$	de Ugarte Postigo et al. (in prep.)
		SMA	3.774	345.0	$4.20 \pm 1.00$	de Ugarte Postigo et al. (in prep.)
SMA	4.775	345.0	$< 4.20 (3.40 \pm 1.40)$	de Ugarte Postigo et al. (in prep.)		
100621A	0.54	APEX	1.500	345.0	$30.00 \pm 6.00$	Greiner et al. (in prep.)
		APEX	2.500	345.0	$13.00 \pm 4.10$	Greiner et al. (in prep.)
		APEX	4.500	345.0	$< 12.00 (3.20 \pm 4.00)$	Greiner et al. (in prep.)
100814A	1.44	APEX	1.138	345.0	$< 4.80 (-0.30 \pm 1.60)$	<a href="#">de Ugarte Postigo et al. 2010a</a>
100901A	1.41	SMA	1.875	345.0	$< 2.25 (0.00 \pm 0.75)$	<a href="#">de Ugarte Postigo et al. 2010e</a>
110106A	—	CARMA	0.069	92.0	$< 2.46 (0.00 \pm 0.82)$	<a href="#">Zauderer et al. 2011b</a>
110205A	2.22	CARMA	0.135	93.0	$< 0.60 (0.00 \pm 0.20)$	<a href="#">Zauderer et al. 2011a</a>
		SMA	0.179	230.0	$< 1.65 (0.00 \pm 0.55)$	<a href="#">Petitpas et al. 2011</a>
110422A	1.77	SMA	13.596	234.0	$< 8.40 (0.00 \pm 2.80)$	Huang et al. (in prep.)
110503A	1.61	SMA	0.454	225.0	$< 5.10 (0.00 \pm 1.70)$	<a href="#">de Ugarte Postigo et al. 2011f</a>
110709B	—	APEX	2.062	345.0	$< 6.90 (1.40 \pm 2.30)$	<a href="#">de Ugarte Postigo et al. 2011d</a>
110715A	0.82	APEX	1.482	345.0	$10.40 \pm 2.40$	<a href="#">de Ugarte Postigo et al. 2011e</a>
		ALMA	3.570	345.0	$4.90 \pm 0.60$	
110719A	—	SMA	0.408	345.0	$< 2.10 (0.00 \pm 0.70)$	<a href="#">Zauderer et al. 2011c</a>
110918A	0.98	APEX	2.290	345.0	$< 15.00 (0.00 \pm 5.00)$	<a href="#">de Ugarte Postigo et al. 2011c</a>

**Notes.** Epochs are given as mid-observing time since the GRB onset ( $t - t_0$ ) or the closest value available. Errors are  $1\sigma$ , while upper limits are  $3\sigma$ . Whenever possible we specify the formal measured flux at the position of the afterglow for detection limits in brackets, when not available we have written 0.00. For observations performed more than 6 months from the burst, obtained to look for the host and not for the afterglow, we do not give the epoch and just mark them as “Late”. <sup>(a)</sup> The detection of GRB 990123 at 353 GHz is probably due to a statistical fluctuation ([Galama et al. 1999](#)). <sup>(b)</sup> The detections of GRB 010222 at 250 and 350 GHz are due to the host galaxy ([Frail et al. 2002](#)). <sup>(c)</sup> The detection of GRB 050408 at 232 GHz is probably due to a statistical fluctuation ([de Ugarte Postigo et al. 2007](#)).